

Article Information



Article Type:	research-article
Journal Title:	Mechanics Based Design of Structures and Machines
Publisher:	Taylor & Francis
DOI Number:	10.1080/15397734.2023.2234466
Volume Number:	0
Issue Number:	0
First Page:	1
Last Page:	25
Copyright:	© 2023 Taylor & Francis Group, LLC
Received Date:	2023-2-19
Revised Date:	2023-6-8
Accepted Date:	2023-7-4
↑	

This is an Accepted Manuscript version of the following article, accepted for publication in Sancibrian, R., Lombillo, I., Sanchez, R., & Gaute-Alonso, A. (2023). Estimation of the static bending modulus of elasticity in glulam elements by ultrasound and modal-updating NDT techniques. *Mechanics Based Design of Structures and Machines*, 52(7), 4642–4666. <https://doi.org/10.1080/15397734.2023.2234466>. It is deposited under the terms of the Creative Commons Attribution-NonCommercial-NoDerivatives License (<http://creativecommons.org/licenses/by-nc-nd/4.0/>), which permits non-commercial re-use, distribution, and reproduction in any medium, provided the original work is properly cited, and is not altered, transformed, or built upon in any way.

Estimation of the static bending modulus of elasticity in glulam elements by ultrasound and modal-updating NDT techniques

Left running head: R. SANCIBRIAN ET AL.

Short title : Mechanics Based Design of Structures and Machines

[AQ0](#)



 Ramon Sancibrian^a[AQ8](#),  Ignacio Lombillo^a,  Rebeca Sanchez^a,  Alvaro Gaute-Alonso^a



^aDepartment of Structural and Mechanical Engineering, University of Cantabria, Santander, Spain

Footnotes

Communicated by Seonho Cho

Corresponding Author

CONTACT Ramon Sancibrian [**AQ9**sancibrr@unican.es](mailto:sancibrr@unican.es)

Abstract

~~Nowadays, glulam timber is becoming a widespread type of structural element due to its economical, mechanical, and ecological properties.~~ Glulam timber is gaining popularity as a structural element due to its cost-effectiveness, strength, and environmental benefits. However, being an organic material, it is susceptible to degradation, ~~unlike other materials.~~ Therefore, nondestructive testing (NDT) methods are essential for assessing its structural health. In this study, two NDT approaches, ultrasound-based and modal updating, were used to predict the static bending modulus of elasticity (MOE) in Pinus Sylvestris and Spruce species. The results demonstrated that the modal updating and linear regression models outperformed the ultrasound technique in accurately determining the static MOE. Additionally, considering the influence of knots improved the accuracy of ultrasound predictions. ~~However, its organic nature causes degradation processes that do not exist in other materials. This fact makes the in-situ inspection of this material~~

extremely important and creates the necessity of developing nondestructive testing (NDT) for structural health assessment. In this work, two NDT approaches, namely an ultrasound-based technique and a modal-updating one are used to predict the static bending modulus of elasticity (MOE) in *Pinus Sylvestris* and Spruce species. To this end, the dynamic modulus of elasticity of 49 samples with three different configurations was determined using the two NDT approaches. The results enable the comparison of the dynamic MOEs with the static ones using the EN 408 European Standard. Simple and bivariate linear regressions are used to obtain the prediction models for the static MOE. The accuracy of the predictive capacity of these models was statistically assessed using the ANOVA test and covariance analysis. Different numerical models were used to study the influence of the non-homogenous MOE in wood. The authors propose implementing substructure-based finite element models and a particle swarm optimization (PSO) algorithm for the modal-updating approach. The results show that the static MOE provided through modal-updating and simple linear regression models significantly improves the results obtained from the ultrasound technique. Furthermore, the consideration of the influence of the knots, by means of the Clustering Knot Density Ratio (CKDR), improves the accuracy of the ultrasound predictions. [AQ1](#)

KEYWORDS

Glulam; modal updating; structural dynamics; nondestructive tests; ultrasound



Note: Any change made here needs to be made in the corresponding section at the end of the article.

This work was supported by the Spanish Ministry of Science and Innovation (Spain) under Grant number TED2021-131522B-I00.

1. Introduction

It is evident that ecological and sustainable construction has become a growing trend in recent decades, and the use of environmentally responsible materials is a fundamental part of this process. Since wood is a sustainable resource that nature provides, the use of timber structures in construction is one of most effective ways to achieve environmental goals (Foster and Reynolds 2018; Cuadrado et al. 2015). Glued laminated timber, also known as Glulam, is a structural product that offers the ecological benefits of wood while enhancing the mechanical properties of sawn timber structures. This makes Glulam an ideal and reliable material for construction. Glulam beams are formed by lamellas, which are pieces of sawn timber glued together by an adhesive between surfaces. This configuration provides high strength, enabling large spans, with different shapes, to build beautiful structures with the natural finish of wood. Despite its numerous technical and environmental advantages, the organic origin of this material introduces multiple factors that may cause its deterioration and reduce its durability (López et al. 2014). Regardless of the preventive treatments received, timber is exposed to numerous degradation processes that are not present in other construction materials (Momohara, Sakai, and Kubo 2021). The deterioration of the material can be caused by abiotic (e.g. water, solar radiation, etc.), biotic (e.g. xylophagous fungi, insects, etc.), and mechanical factors (e.g. deformations, breaks, mechanical overstress, etc.). The presence of damage and defects reduces the strength and stiffness of glulam structures and, for this reason, the use of nondestructive tests (NDT) is necessary for in-situ inspection.

The modulus of elasticity (MOE) of glulam elements has a direct relationship with the strength properties and its determination is an accurate source of information about the reliability of these structures (Cavalli et al. 2016; Z. Zhang, Li, and Yang 2021). However, wood is a heterogeneous, hygroscopic, and anisotropic material and its mechanical properties depend on many factors. This means that NDT techniques used in other materials must be adapted to the special characteristics of this material. Several methods have been proposed for assessing the health status of timber structures, including visual grading (Arriaga et al. 2022) and methods based on technologies such as ultrasound (Neuenschwander et al. 2013), dynamic response (Genç et al. 2021; C. W. Zhang 2023), penetration resistance (Palma and Steiger 2020), etc. Technological methods provide physical variables that can be related to MOE, both static and dynamic (Z. Zhang et al. 2022). Visual grading is perhaps the least technological method, but it is the most widely used. This is because methods based on the measurement of the physical properties are not considered accurate enough to provide reliable results (Sousa et al. 2013). In fact, due to the uncertainties present in the material, it is often difficult to relate the data obtained from the measurements to the strength and stiffness properties of glulam components. This lack of confidence is due to the presence of natural defects, such as knots, cracks or voids, making timber elements a non-homogeneous material with a random variation in mechanical properties throughout the structural components. As a consequence, it becomes necessary to combine different NDT methods, including visual grading and other techniques based on the physical measurement of variables. This requires looking at the experimental results as a whole to obtain a full picture of the situation, making subjective decisions about the reliability of the structures in which the engineering judgment and expertise play an important role.

Ultrasound testing is a nondestructive technology used for the assessing structural components (Chen and Li 2022; Liu et al. 2023). The propagation of waves through material is generated by a piezoelectric sensor and involves the analysis of the signals transmitted to the receiver. The transducers are located in different parts of the structural elements and the changes in the transmitted waves are related to the presence of damage or deterioration. The application of ultrasound techniques to timber has been applied since the 1980s (Wilcox 1988). However, ultrasound wave propagation in timber is difficult to predict due to the anisotropic feature of this material. For instance, wave propagation differs between the longitudinal and transversal directions. The common way to assess stiffness in timber is the determination of the wave velocity in the longitudinal direction (Kovryga, Khaloian Sarnaghi, and van de Kuilen 2020). Transverse ultrasound waves are used to detect small defects such as cracks, splits, etc (Kabir, Schmoldt, and Schafer 2002). However, the presence of defects is not the only factor modifying ultrasound wave propagation in wood's structure, but so do moisture content and different types of natural discontinuities (e.g. knots, bark pockets, waness, grain deviation, etc.) (Tiitta et al. 2017). Due to these uncertainties, the relation between the dynamic and static MOE is not fully understood in the literature (Fathi, Kazemirad, and Nasir 2021). As a consequence, NDTs based on ultrasound measurement fails to obtain an accurate estimation of the static MOE from the dynamic one. In the literature, several authors suggested the use of correction factors to estimate the MOE from ultrasound measurements (Ettelaoui et al. 2019). However, it is evident that developing a NDT technique for MOE estimation in glulam is a challenge that remains unresolved.

On the other hand, vibration-based nondestructive methods have been applied to determine the dynamic MOE

in several studies, including timber and other types of structures (Altunışık, Okur, and Kahya 2017). These methods are based on the loss of stiffness caused by damage to the material. Damage affects the dynamic parameters (damping, mass, and stiffness) and consequently alters the modal characteristics such as natural frequencies and mode shapes (Z. Q. Lu et al. 2020). By comparing the modal characteristics of the healthy system with the actual structural model, these changes can be utilized for structural diagnosis (Z.-Q. Lu et al. 2022; Barroso and Rodriguez 2004). In the last decades, several methods have been proposed based on this concept. For instance, methods based on modal frequency-strain energy relationship (Hu et al. 2006), measurement of the Frequency Response Function (FRF) and wavelets (Qu, Li, and Chen 2019), autoregressive approaches (Doebeling, Farrar, and Prime 1998), and based on derivatives (Whalen 2008). The most commonly used damage identification and location methods are those based on the changes in natural frequencies (Sun et al. 2022). This is because natural frequencies are sensitive to variations in stiffness caused by damage or deterioration and are easily measured and identified in modal analysis. However, when uncertainties exist in multiple variables, relying on natural frequency variations alone may not be sufficient for accurate identification. In fact, more complex problems require the incorporation of mode shapes in the diagnostic analysis. The determination of the changes of natural frequencies and mode shapes is carried out by finite element modal updating. This technique enables the comparison of the dynamic behavior of the structural component and the simulated response obtained from a finite element model (FEM) (Altunışık et al. 2019). The analysis of the discrepancies between measurements and simulated response enables the identification of the variations in stiffness and damage. To this end, a goal function and a minimization process need to be formulated to reduce the differences in modal characteristics between the finite element model and the experimental data. The complexity of minimization depends on the number of variables involved in the problem. Local search optimization could be sufficient for easy problems. However, when dealing with a high number of variables, evolutionary computation (EC) approaches become necessary. Genetic Algorithms (GA) (Tang, Ye, and Huang 2023), Differential Evolution (DE) (Perera, Marin, and Ruiz 2013), and Particle Swarm Optimization (PSO) (Alkayem, Cao, and Ragulskis 2019) are remarkable EC approaches applied to finite element model updating.


In this study, the static bending MOE is regarded as the key parameter for evaluating the health status of the structural systems. Therefore, the main goal of this work was to obtain prediction models of the static bending MOE obtained from two NDT techniques for glulam components. The NDT techniques were modal analysis and ultrasound measurement. Although the application of these NDT techniques in sawn timber is extensively documented in the literature, there is a lack of knowledge in predicting the static MOE in glued laminated timber (Sanabria et al. 2015). To this end, 49 samples have been tested and analyzed following three steps. Firstly, the standardized four-point bending test was used to obtain the actual static MOE of each sample. Secondly, ultrasound and modal-updating NDT techniques were used to obtain the dynamic MOEs. To take into account the non-homogeneity features of glulam, the paper proposes the use of a particle swarm optimization (PSO) approach based on substructured models for finite element modal updating. Finally, the correlation between static and dynamic MOEs is presented in the paper. Different types of models, namely simple linear regression (SLR) and bivariate linear regression (BLR), were generated to assess the influence of

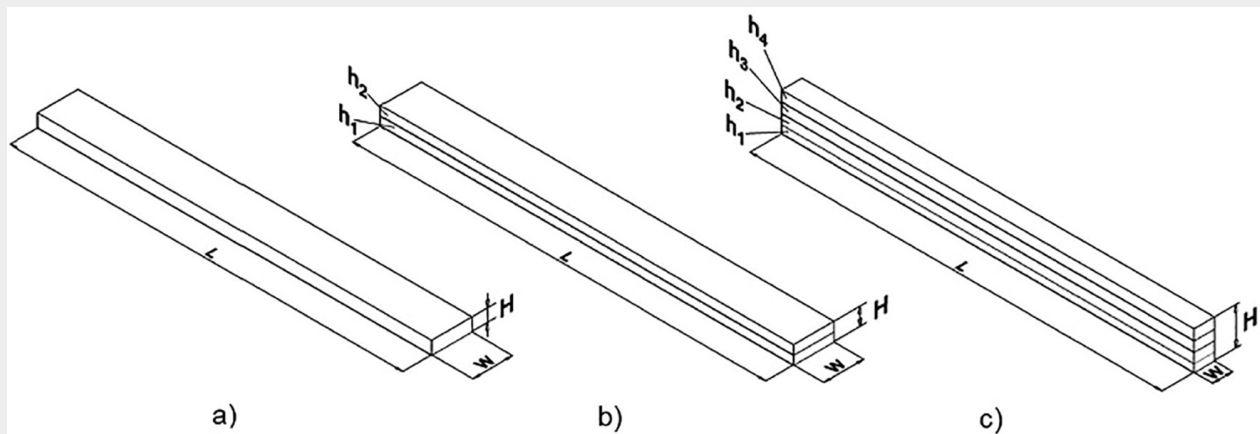
the density and concentration of knots. The adequacy of the models and their accuracy were compared and evaluated using the ANOVA test and covariance analysis.

2. Materials and methods

2.1. Sample description

In this section, the samples used in the experimental trials are described. A total of 49 samples of *Pinus Sylvestris* and Spruce species from northern Europe were tested in three different configurations, which were: single beams (see Fig. 1a), duo-laminated beams (see Fig. 1b), and glulam beams (Fig. 1c).

Figure 1. Samples used in the tests: (a) Simple, (b) duo-laminated, and (c) glulam beams. 



Single beams are sawn timber or lamellas used to produce glulam beams. They were first tested in order to obtain the mechanical characteristics of the individual elements, which will be forming part of the Glulam beams. Duo-laminated beams consist of two lamellas joined together by a layer of MUF adhesive (Melamine Urea Formaldehyde). These samples provide the mechanical characteristics of the simplest glulam element and are used to evaluate the influence of the combined configuration. Finally, four-lamellas glulam beams were tested to obtain information about the behavior of a real beam configuration and compare the results with the other two setups. The grading class were C18, C24 and C30 for single and duo-laminated samples, and GL24 and GL28 for glulam beams (European Standard EN 14081-14081:2020). They were stored in the laboratory under stable conditions of temperature and humidity. The weight of each sample was measured and used to obtain its global density. The dimensions of the different types of sample beams are quite similar, showing only small deviations. The geometrical dimensions and density values are shown in Table 1 according to the nomenclature used in Fig. 1. The parameters presenting geometrical and density variations between samples are shown in Table 1 by using the mean value and standard deviation (SD).


Note: The table layout displayed in 'Edit' view is not how it will appear in the printed/pdf version. This html display is to enable content corrections to the table. To preview the printed/pdf presentation of the table, please view the 'PDF' tab.

Table 1. Main features of the samples tested. 

Beam type	Specie	Samples	Lamellas	Density (kg/m ³)	Dimensions (m). Mean (SD)						
					L	W	H	h1	h2	h3	h4
Single	Pinus S.	14	1	506.6 (58.44)	1.57 (0.021)	0.16 (0.013)	0.05 (0.004)	–	–	–	–
	Spruce	14	1	459.3 (49.73)	1.57 (0.025)	0.16 (0.012)	0.05 (0.005)	–	–	–	–
Laminated duo	Pinus S.	12	2	484.1 (24.40)	1.65 (0.021)	0.16 (0.013)	0.07 (0.004)	0.04	0.03	–	–
	Spruce	5	2	470.4 (25.36)	1.74 (0.025)	0.13 (0.012)	0.07 (0.005)	0.04	0.03	–	–
Glulam	Pinus S.	2	4	552.93	1.65	0.08	0.15	0.04	0.04	0.04	0.03
	Spruce	2	4	459.46	1.65	0.08	0.15	0.04	0.04	0.04	0.03

Place the cursor position on table column and click 'Add New' to add table footnote.

2.2 Visual grading

Following the European Standard EN 1309-3 (2018^{}) all the samples were examined in search of defects, singularities, and possible biological degradation. The result of the examination confirmed that there are no major defects that would lead to a significant deviation from the expected behavior. The six sides of each sample were photographed and recorded in a database. The presence of knots and clustered knots was evaluated by their size in the six faces of each sample. It was evaluated using the Concentrated Knot Diameter Ratio (*CKDR*) (Divós and Tanaka 2005),

$$CKDR = \frac{\sum d_i}{2(W + H)}$$

(1)


This equation measures the proportion of the cross-section occupied by the knots by calculating the sum of the knot diameters (d_i) divided by the sum of the width (W) and depth (H) of the sample. The $CKDR$ factor is evaluated every 15 cm along the main axis of the sample. The maximum value of $CKDR$ provides the quality of the sample. Other features such as the existence of resin pockets, the slope of grain, waness, and cracks were evaluated and registered according to the aforementioned standard.

2.3. Obtaining the bending modulus of elasticity

The bending Modulus of Elasticity is a mechanical property that characterizes the stiffness of the material. Therefore, a reduction in the MOE usually indicates the presence of defects or the deterioration of the mechanical properties of the material. Thus, the knowledge of MOE is an essential factor in determining the health status of glulam structures. However, the accurate in-situ measurement of MOE is not an easy issue when NDT techniques are required. In this work, the MOE is determined by three methods, which are: (1) static bending tests (E_{ST}), (2) direct ultrasound (E_{US}), and (3) modal updating (E_M).

The E_{ST} is obtained in the laboratory and it is considered the most accurate method out of the three. However, it is impracticable in-situ and, for this reason, it cannot be used as a NDT technique in determining the health status of the structure. In this work, it was considered as a reference value for the MOE, which provides knowledge of the actual state of each sample. Static Modulus of Elasticity (E_{ST}) was obtained by performing a bending test in each sample in accordance with the European Standard EN 408-408 (2011). Thus, four-point bending tests were performed in the main strength direction, see Fig. 2, progressively loading the specimen and using a linear variable differential transformer (LVDT) for measuring deflections at the midspan. The static modulus of elasticity can be obtained according to the aforementioned standard as follows,

$$E_{ST} = \frac{3aL^2 - a^3}{2WH^3 \left(2 \frac{\Delta\delta}{\Delta F} \right)}$$

Figure 2. Four-point bending test carried out in laboratory for the determination of. E_{ST} 



Where a is the distance from the load to the nearest support in the bending test, $\Delta\delta$ is the increment in the deflection at the midspan for the increment of the load ΔF , according to the standard procedure.

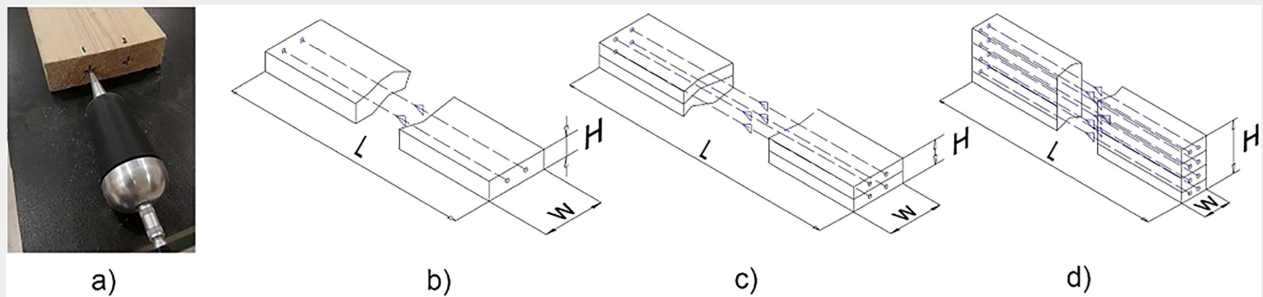
Alternatively, direct ultrasound measurements were used to obtain the dynamic Modulus of Elasticity (E_{US}). The ultrasound measurements were carried out using a Sylvatest Trio device, which comprises two ultrasonic piezoelectric transducers (i.e., one emitter and one receiver) working together at a frequency of 22 kHz. The transducers have a conical shape with a cylindrical pin at the end. In order to perform the measurements, the pin is inserted into a small drilled hole made at both ends of each sample. The time of flight (ToF) of ultrasonic waves is measured from emitter to receiver to obtain the velocity of propagation V_{US} of the waves through the timber specimen. The dynamic Modulus of Elasticity is determined using the one-dimensional wave as outlined in Bucur (2006),

$$E_{US} = \rho V_{US}^2 = \rho \left(\frac{L}{ToF} \right)^2$$

where L is the specimen length and ρ is the density of the material.

Figure 3(a) shows the transducer coupled to the specimen ready for measurement. In all samples, two measurements of the ToF were performed in each lamella. The two points at each end indicating the measurement location in single specimens are shown in Fig. 3(b). For duo-laminated samples, four measurements were carried out (Fig. 3c), and eight values were obtained for glulam samples (Fig. 3d). This procedure provided the modulus of elasticity in each lamella from the mean value of the two ToF measurements.

Figure 3. Performance of ultrasound measurements. Positions of the holes to connect the ultrasound transducers at the lamellas ends: (a) cone-shaped transducer coupled ready for the measurement, (b) simple beams, (c) laminated-duo beams, and (d) glulam samples. +



A model updating procedure based on experimental modal analysis (EMA) and an optimization algorithm for the determination of the dynamic modulus of elasticity (E_M) were developed in this work. The methodology is based on the determination of the specific natural frequencies and mode shapes that each specimen possesses depending on its elastic modulus, density, and geometry. In this process, an input vibration is generated to determine the E_M by exciting the specimen with a bending impulse. A cantilever beam setup was selected as a representative glulam structure. This is because the boundary conditions are easily controlled fulfilling requirements of repeatability and reproducibility. An adjustable metal support was constructed to clamp the specimens on a rigid wall. [Figure 4](#) shows the setup for measuring the natural frequencies and mode shapes in the three types of specimens. The transducers used are four capacitive accelerometers (Kistler 8316 A) with a frequency range from 0 Hz to 1 kHz and dynamic amplitude from 0 g to 10 g. The accelerometers were evenly distributed along the main axes of the specimen. Double-sided adhesive tape was used for mounting the accelerometers. A piezoelectric impulse force hammer was used for the excitation of the systems (Kistler 9724 A) with a force range from 0 N to 2000 N. The signals from the accelerometers and the hammer were acquired through a measuring amplifier (HBM, QuantumX MX1601B) with a maximum sample rate of 20 kHz per channel. Modes and resonant frequencies were obtained using commercial software for experimental modal analysis (ARTEMIS Modal v7.2). The roving hammer test was performed by impacting on four locations close to the accelerometers' positions. The signals coming from accelerometers and the hammer were analyzed to isolate the modes and resonant frequencies using the Rational Fraction Polynomial with complex Z mapping (RFP-z) and the Complex Mode Indication Function (CMIF) (Sun et al. [2022](#)). The sampling frequency was set to 1200 Hz using an antialiasing filter. [Figure 5](#) shows the setup used in one test carried out in this work for the modal analysis of a duo-laminated sample.

Figure 4. Cantilever setup used to obtain the E_M by using modal updating technique in (a) single, (b) duo-laminated, and (c) glulam specimens. +

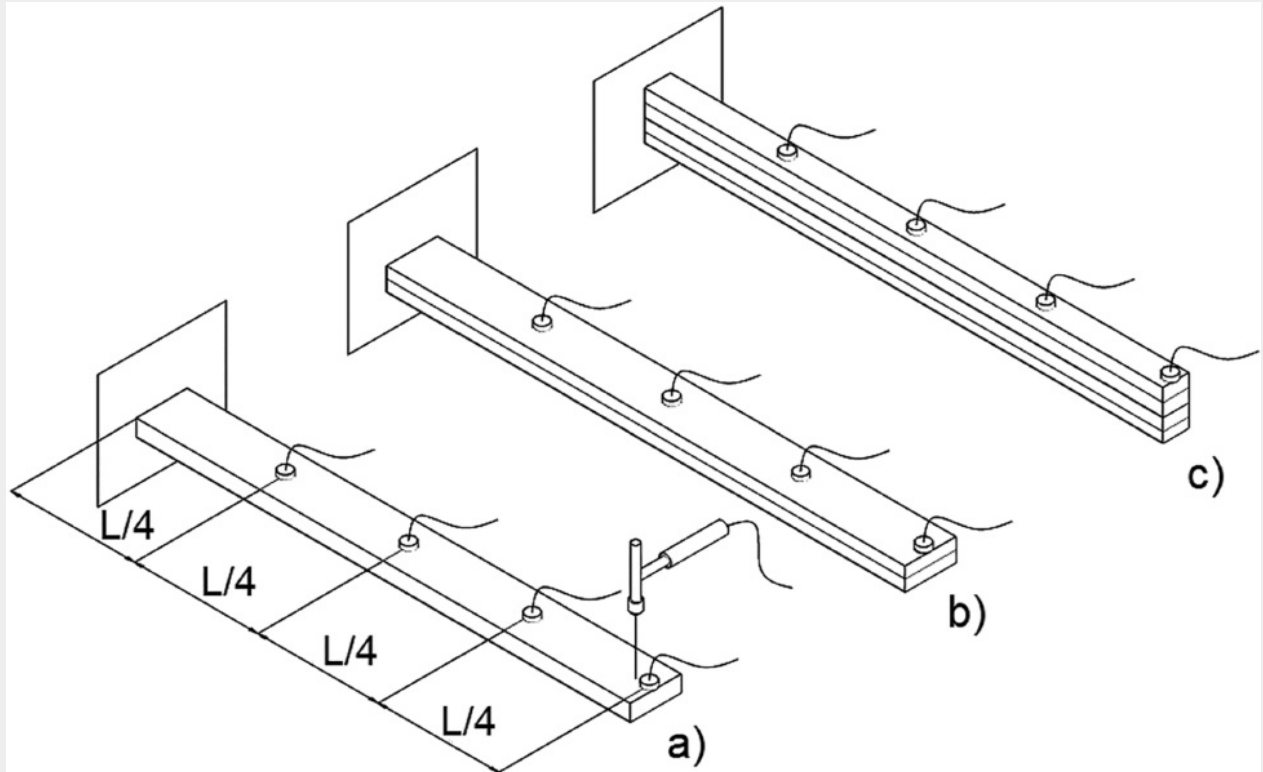

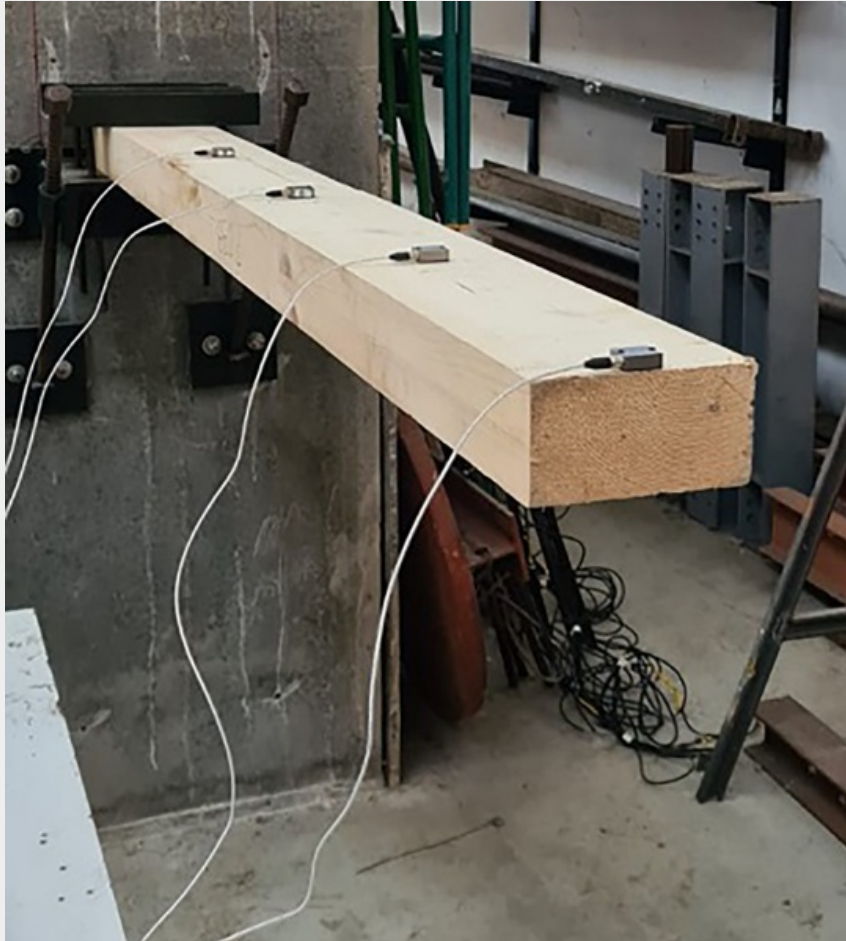


Figure 5. Cantilever duo-laminated sample ready for modal analysis. 




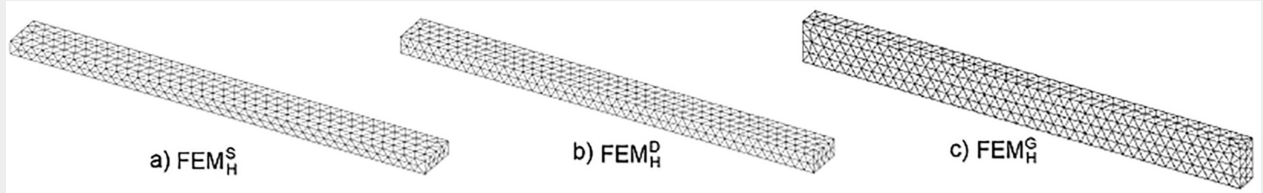
The determination of the moisture content (MC) in the samples was performed using the electrical resistance method (European Standard EN 13183-22 [2002](#)). A measuring meter for structural wood moisture (GANN Hydromette RTU 600) was used during the experiments. The moisture content was measured in each lamella just before the samples were tested. In all cases, density and elasticity modulus were normalized to 12% humidity according to the European Standard EN 384:2016 ([2020](#)¹⁰).

2.4. Determination of the MOE using modal updating in homogeneous finite element models based on local search optimization

For modeling all the specimens tested, 3D homogeneous finite element models formed by quadratic tetrahedral elements were created in Matlab[®]. In this context, homogenous indicates that the bending modulus of elasticity is constant along the whole specimen. These theoretical models were employed for both static and dynamic

simulation of the beams. The static analysis was performed to compare the static bending stiffness of the theoretical models with the results obtained from the experimental tests (E_{st}). On the other hand, finite element dynamic analysis was used to update the models by comparing the natural frequencies extracted from the experimental modal analysis with those frequencies obtained from the theoretical models. The geometry and meshing of the three different finite element models can be observed in Fig. 6. The finite element models are named FEM with a superscript indicating the type of beam (i.e., S for single beams, D for duo-laminated beams, and G for glulam beams), with subscript H denoting the homogeneous properties of the model. The meshing of the homogeneous single beam (FEM_H^S) is formed by 1301 elements. The homogeneous duo-laminated beam model (FEM_H^D) is formed by 4287 elements, and the model for glulam beams (FEM_H^G) contains 2359 elements. The assumptions made for these finite element models are as follows: (1) the material is homogeneous and isotropic, (2) the lamellas are perfectly bonded to each other in duo-laminated and glulam specimens, (3) a perfect clamp (fixed support) is applied as the boundary condition at the beam end, and (3) the effect of damping is disregarded.

Figure 6. Homogeneous FEMs for (a) single, (b) duo-laminated, and (c) glulam specimens. 



In the numerical model, the natural frequencies are obtained by solving the eigenvalue and eigenvector problem represented as,

$$(\mathbf{K} - \mu \mathbf{M})\Phi = 0$$

In this equation, \mathbf{K} represents the stiffness matrix, \mathbf{M} represents the mass matrix, Φ corresponds to the eigenvectors or modes, and μ contains the eigenvalues that include the squared natural frequencies along the main diagonal.

Assuming that $\Phi \neq 0$, a non-trivial solution exists in Eq. (4) leading to,

$$\det(\mathbf{K} - \mu\mathbf{M}) = 0$$

By solving this equation, the natural frequencies ω_i can be obtained. The mode shapes can be determined by substituting the natural frequencies into [Eq. \(4\)](#) and solving the resulting system of equations.

In this work, the first four natural frequencies and mode shapes are used to update the modes. This information is expressed as follows,

$$[\mathbf{\Omega}_p \quad \mathbf{\Phi}_p]_H^{typ} = \begin{bmatrix} \omega_1 & \phi_{11} & \phi_{12} & \phi_{13} & \phi_{14} \\ \omega_2 & \phi_{21} & \phi_{22} & \phi_{23} & \phi_{24} \\ \omega_3 & \phi_{31} & \phi_{32} & \phi_{33} & \phi_{34} \\ \omega_4 & \phi_{41} & \phi_{42} & \phi_{43} & \phi_{44} \end{bmatrix}_{mod}^{typ}$$

Here, $\mathbf{\Omega}$ is the vector containing the natural frequencies, $\mathbf{\Phi}$ represents the mode shapes, and subscript p denotes whether it is from experimental ($p = e$) or theoretical ($p = t$) data. The terms ϕ_{rs} stand for the components of the normalized mode shapes, where subscript r is the mode number and s is the component assigned to the measurement point or degree of freedom. The superscript typ indicates the type of specimen (i.e., S = single, D = duo-laminated, or G = glulam). The subscript H refers to the homogeneous theoretical model.

The comparison of the natural frequencies is given by,

$$F(E_{MH}) = \frac{1}{2} \sum_{i=1}^m \tau_i \left(\frac{\omega_{ti} - \omega_{ei}}{\omega_{ei}} \right)^2$$

Here, ω_{ti} and ω_{ei} denote the natural frequencies obtained from the theoretical and experimental models, respectively. The parameter m is the number of modes considered (i.e., $m = 4$), and τ_i is the weighted

parameter assigned to each mode. The design variable is E_{MH} , [The comma "," is not part of the equation.] which corresponds to the homogeneous dynamic modulus of elasticity. If the result given by Eq. (7) is less than a threshold β , [The comma "," is not part of the equation.] the modulus of elasticity E_{MH} is considered the solution (i.e., E_{MH}^*). In this work $\beta = 1e-4$. If this condition is not fulfilled in the first iteration (which is common in most cases) the optimization process starts by optimizing the goal function depicted Eq. (7). This optimization process is based on gradient descent determination using the following equation,

$$E_{MH}^{k+1} = E_{MH}^k - \alpha \nabla F(E_{MH}^k)$$

where α is the stepsize, which is obtained by well-known methods used in optimization, and the gradient is calculated using (Haftka Raphael T. 1992),

$$\frac{d\mu}{dE} = \varphi^T \frac{dK}{dE} \varphi$$

where φ are the normalized mode shapes (to simplify the notation during the derivation, the subscripts and superscripts have been omitted). The derivatives of the squared natural frequencies in the main diagonal are determinate as,

$$\frac{d(\omega_t^2)}{dE} = \text{Diag}\left(\frac{d\mu}{dE}\right)$$

and the natural frequencies are obtained from,

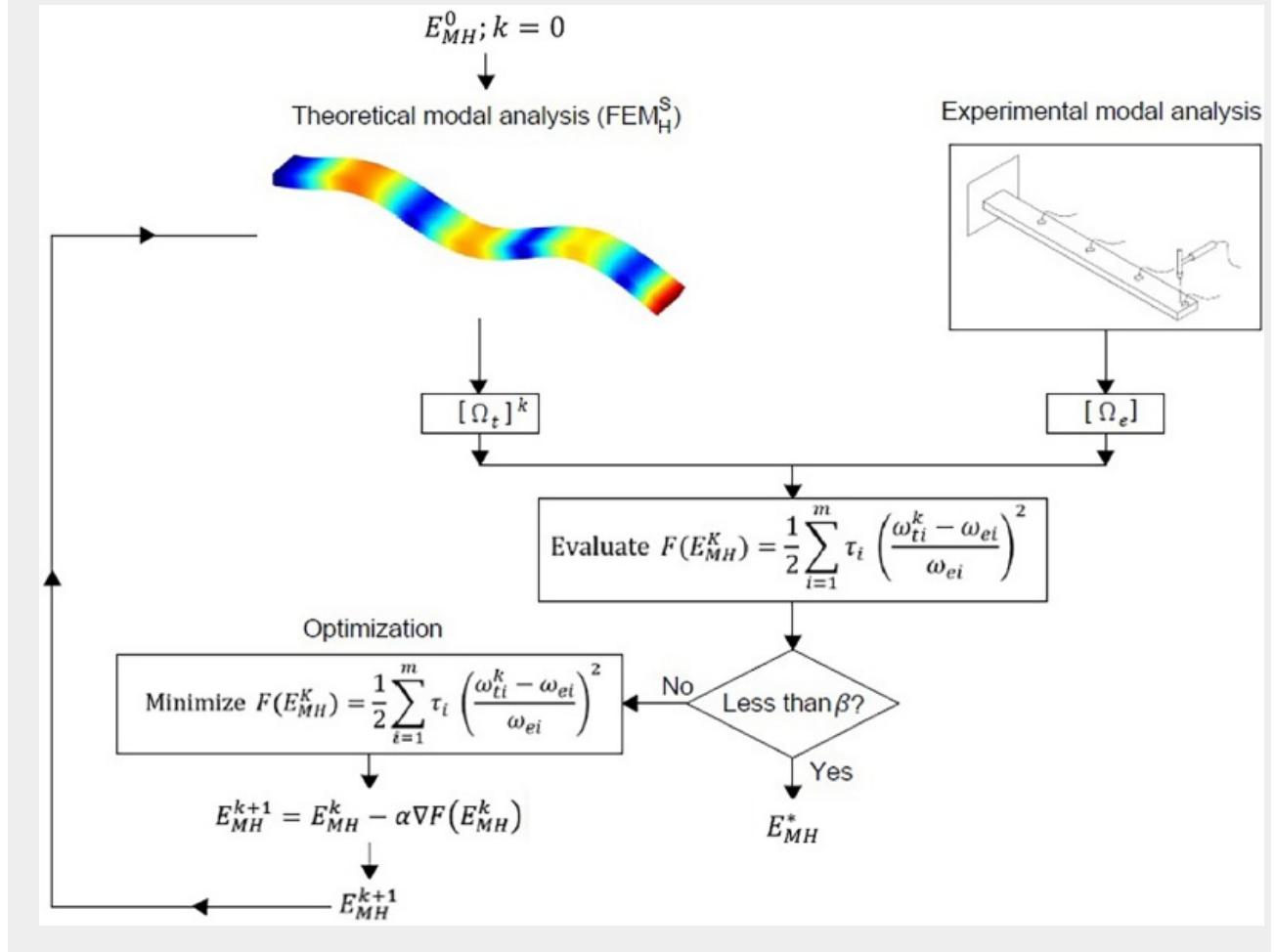
$$\frac{d\omega_{ti}}{dE} = \frac{1}{2\omega_{ti}} \frac{d(\omega_{ti}^2)}{dE}$$

Finally, the gradient in each iteration is given by,

$$\nabla F\left(E_{MH}^k\right)=\sum_{i=1}^m \tau_i \frac{d \omega_{t i}}{d E}\left(\frac{\omega_{t i}-\omega_{e i}}{\omega_{e i}}\right)$$

which is introduced into [Eq. \(8\)](#) allowing the determination of the next dynamic modulus of elasticity in the iterative process. This process is repeated until the comparison yields a result lower than the threshold β . The optimum solution (i.e., E_{MH}^*) is thus obtained, representing the dynamic modulus of elasticity that best fits the experimental natural frequencies in the numerical model. The whole optimization process is depicted in [Fig. 7](#).

Figure 7. Finite element model updating by means of the optimization procedure +




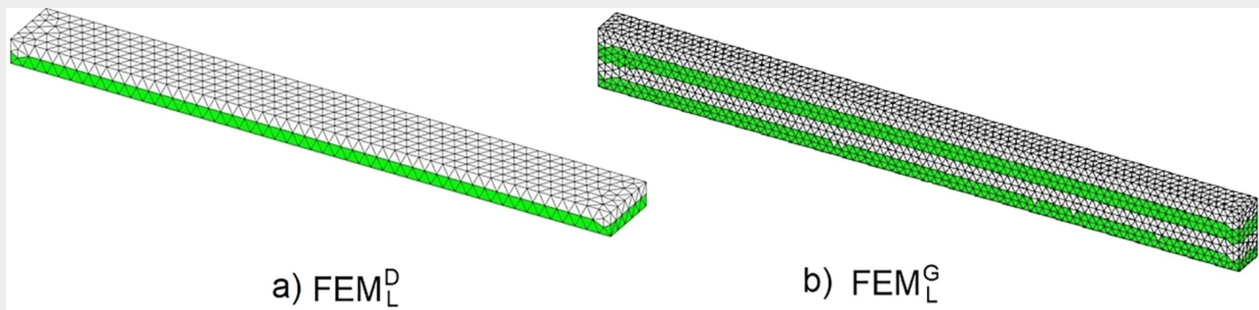
2.5. Determination of the MOE using modal updating based on Particle Swarm optimization (PSO) in non-homogeneous finite element models

The finite element models presented in the previous section considered the elasticity modulus as a homogeneous variable for bending strength. However, due to the organic origin of timber, there is more likely to be a significant variability in the mechanical properties in each specimen. These differences could be local or global. For instance, global changes in MOE are due to the different elasticity modulus between lamellas forming the glulam specimen, and local effects are due to the presence of defects and/or natural discontinuities (e.g. knots, bark pockets, waness, grain deviation, etc.).

In this work, a finite element model-updating technique based on substructures was implemented to find the

variation of MOE throughout the different lamellas. The finite element model enables different values of the MOE to be assigned to the different wooden boards (also called substructures). The correct assignation of a MOE to these substructures should allow a better fit of natural frequencies and mode shapes than that obtained with the homogeneous models. Figure 8 shows these models for duo-laminated (Fig. 8a) and glulam (Fig. 8b) specimens, where the substructures are emphasized in colored zones. In this case, the subscript L stands for the numerical model with the lamellas modeled as substructures. Thus, the colors green and white differentiate the substructures with different MOEs. Zones with uniform color have homogeneous stiffness values. However, it is important to highlight that substructures in Fig. 8(b) with the same color do not necessarily have the same MOE. The assumptions made for the homogeneous finite element models are still applicable here, with the exception of the homogeneity and isotropy conditions, which obviously do not hold in this non-homogeneous case.

Figure 8. Substructured FEMs of (a) duo-laminated, and (b) glulam beams. 



The objective of these numerical models is to study the influence of the different stiffness properties of each lamella on the global behavior of the beams. Thus, the MOE of these models is denoted as the vector \mathbf{E}_{LM}^D and \mathbf{E}_{LM}^G for duo-laminated samples and glulam beams, respectively. That is,

$$\mathbf{E}_{LM}^D = [E_{LM}^{D1} \ E_{LM}^{D2}]$$

$$\mathbf{E}_{LM}^G = [E_{LM}^{G1} \ E_{LM}^{G2} \ E_{LM}^{G3} \ E_{LM}^{G4}]$$

Assuming that the experimental modal measurements are correct, the differences between the theoretical and experimental model should be minimized by using the following goal function,

$$\text{minimize } F(\mathbf{E}) = \frac{1}{2} \sum_{i=1}^m \tau_i \left(\frac{\omega_{ti} - \omega_{ei}}{\omega_{ei}} \right)^2 + \sum_{i=1}^m \vartheta_i (1 - MAC_i)^2$$

where **MAC** is the Modal Assurance Criterium (Perera and Ruiz 2008), which is frequently applied to measure the differences between the theoretical mode shapes and the experimental ones (Kouroussis, Ben Fekih, and Descamps 2017). The **MAC** value is weighted by the coefficient ϑ_i in the goal function.

Mode shapes are introduced here because the size of the problem requires more information to find accurate solutions. Thus, it is necessary to change the objective function used in single beams by Eq. (15), in order to adapt the algorithm to the new set of design variables. Furthermore, to improve the efficiency and robustness of the optimization process, the Particle Swarm Optimization (PSO) algorithm was used to minimize Eq. (15). Using this approach, the vector of design variables containing the stiffness of each substructure is randomly generated and termed as particles to be optimized in the mathematical process. The PSO algorithm can be mathematically formulated in the following way (Alkayem, Cao, and Ragulskis 2019),

$$\begin{aligned} v_j^{k+1} &= \alpha v_j^k + b_1 r_1 (g_{best\ j} - E_j^k) + b_2 r_2 (g_{best} - E_j^k) \\ E_j^{k+1} &= E_j^k + v_j^{k+1} \end{aligned}$$

In Equation (16), the first part provides the velocity of the particle j , [The comma "," is not part of the equation.] (i.e., v_j^{k+1}) at iteration k . The parameter α is the weight of the inertia, b_1 and b_2 are the so-called acceleration coefficients. The parameters r_1 and r_2 are random numbers generated between 0 and 1. The modulus of elasticity in each substructure at iteration k is E_j^k , [The comma "," is not part of the equation.] which is updated to E_j^{k+1} in the next iteration (i.e., $k+1$) by using the second equation. The best position of particle j at iteration k is $g_{best\ j}$ and the best position of the group up to iteration k is g_{best} . [The period "." is not part of the equation.] These parameters remain fixed throughout the optimization process (in this work these parameters are set as $\alpha = 1.0$, and $b_1 = b_2 = 2.0$).

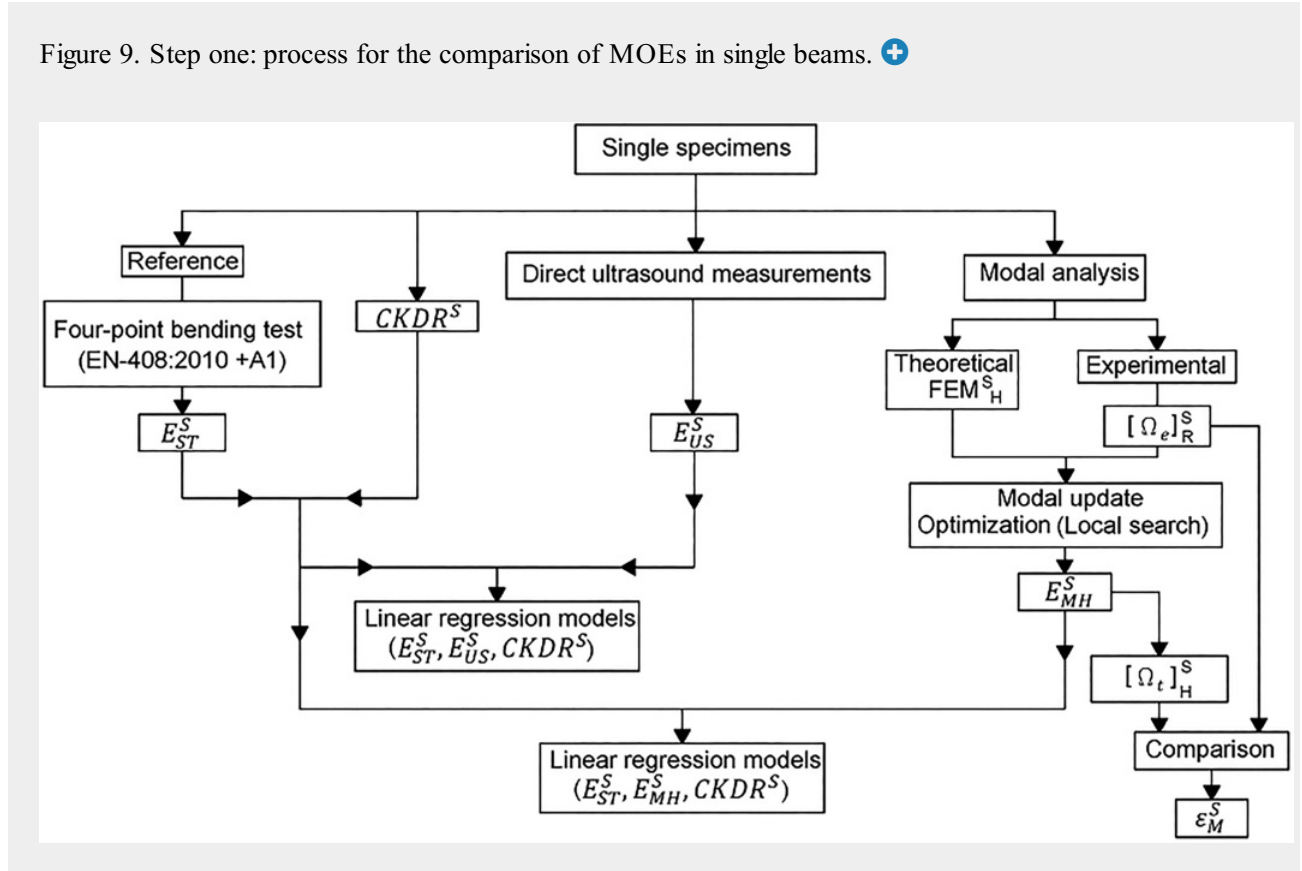
Thus, the iterative process modifies the stiffness values in the FE model assigned to substructures to match the results obtained in the model and the experimental results. The algorithm starts by creating an initial set of particles (vector E_j), which is stored in a matrix with the dimensions coincident with the number of substructures. A fixed number of population size, Np , [The comma "," is not part of the equation.] is established in this work equal to 100 particles. Two stopping criteria are used. The first one is the number of generations, which is limited to a maximum, G_{max} (in this work $G_{max} = 50$ generations). The second one is a threshold in the value of the objective function, in a similar way used in the local search (i.e., $\beta < 1e-4$). The first criterion to be fulfilled establishes the termination of the optimization process.

2.6. Relationship between different MOEs obtained using the different methods

The experimental tests provide the relationship between the MOEs obtained by three different procedures, i.e., the static bending test, ultrasound wave propagation and modal updating. The general procedure consists of three steps conducted on: (1) single beams, (2) duo-laminated beams, and (3) glulam beams. The first step provides the basic relationships between different MOEs in single beams and evaluates the influence of the Concentrated Knot Diameter Ratio (*CKDR*). Thus, it provides the features of this material that will be useful in the next steps. In the second step, the static MOEs of duo-laminated beams are determined and compared with the extrapolated results obtained from single beams. In the third step, the same procedure used with duo-

laminated beams is repeated for the glulam beams in order to obtain information in the current situation. Figure 9 illustrates the procedure carried out in step one for each single beam. The 28 samples of the two species were studied to obtain theoretical and experimental MOEs.

Figure 9. Step one: process for the comparison of MOEs in single beams. +



The experimental static bending modulus of elasticity (E_{ST}^S) was determined according to the European Standard EN-408 (2011) and serves as a reference value for the MOE. The E_{US}^S was obtained by direct ultrasound measurement following the aforementioned procedure. Modal experimental analysis was performed in each single beam to obtain natural frequencies, i.e., $[\Omega_e]^S_R$, where subscript R stands for real system. The local search optimization method was used to update the model FEM_H^S using the objective function shown in Eq. (7), obtaining the bending modulus of elasticity of the homogeneous model, i.e., E_{MH}^S . The comparison of the experimental natural frequencies and those obtained by optimization, i.e., $[\Omega_t]^S_H$, provides an evaluation of the quality of the fit regarding the structural model. The modal error in single beams, denoted as ϵ_M^S is determined through the following equation,

$$\varepsilon_M^S(\%) = \left| \frac{\omega_{ti} - \omega_{ei}}{\omega_{ei}} \right| 100; i = 1, 2, \dots, m$$

where ω_{ei} is the i -th natural frequency obtained by experimentation and ω_{ti} refers to the same value obtained theoretically.

The results obtained from this first step enable the relationship between the MOEs and the influence of the *CKDR* by using statistical regression techniques. As will be verified later, and in accordance with the results obtained by other authors (Fernández-Serrano and Villasante 2021), these relationships are strongly linear. For this reason, they are established as follows,

$$E_{ST}^S = A_1 + B_1 E_{US}^S$$

$$E_{ST}^S = A_2 + B_2 E_{MH}^S$$

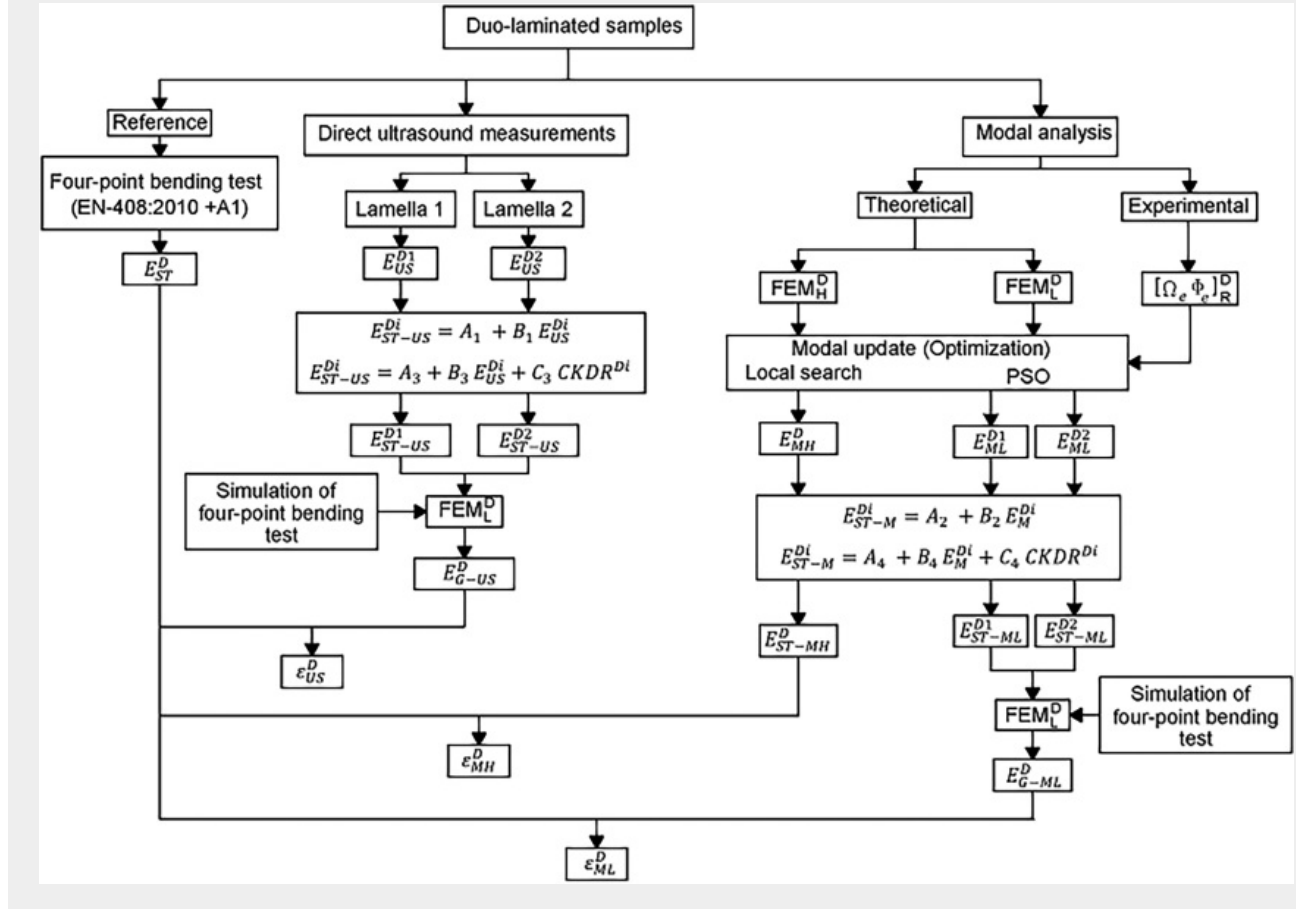
$$E_{ST}^S = A_3 + B_3 E_{US}^S + C_3 CKDR^S$$






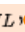
$$E_{ST}^S = A_4 + B_4 E_{MH}^S + C_4 CKDR^S$$

where A , B and C represent the linear regression coefficients. Equations (18) and (19) establish the relationship without considering the influence of knots, whereas Eqs. (20) and (21) include the effect of the $CKDR$. These equations will enable the prediction of the E_{ST}^S from modal and ultrasound MOEs in the next step.

Figure 10 shows the procedure carried out in step two, where the 17 duo-laminated specimens were tested to obtain the MOEs by the three different methods. The E_{ST}^D of the duo-laminated beams was experimentally obtained by using the standardized four-point bending test in a similar way to step one. Ultrasound testing was used to obtain the E_{US}^D in each lamella forming the duo-laminated beam (i.e., E_{US}^{D1} and E_{US}^{D2} by sample). The MOE of each lamella was transformed into the static modulus of elasticity, (i.e., E_{ST-US}^{D1} and E_{ST-US}^{D2}) by using the relationships given by Eqs. (18) and (20). These moduli were used for modeling the stiffness of the substructures (lamellas) in the numerical model $MEFL^D$ depicted in Fig. (a). This model is solved in a static simulation of the standardized four-point bending test to obtain the global static modulus (i.e., E_{G-US}^D) of the duo-laminated beam by using Eq. (2). This modulus can be compared with the same modulus obtained experimentally in the standardized test (i.e., E_{ST}^D). The difference is the error of the ultrasound-based technique for the estimation of the static bending stiffness (i.e., ϵ_{US}^D).

Figure 10. Step 2: comparison of MOEs in duo-laminated beams. 



On the other hand, the experimental modal analysis provides the natural frequencies and mode shapes of the duo-laminated beams, i.e., $[\Omega_e \Phi_e]^D_R$.  [The period "." is not part of the equation.] In order to obtain the bending dynamic modulus of elasticity, the homogeneous (MEF_H^D) and substructured (MEF_L^D) finite element models were updated by means of optimization. In the homogeneous model, the updating process provides E_{MH}^D ,  [The comma "," is not part of the equation.] whereas the substructured models provide one modulus for each lamella forming the beam, i.e., E_{ML}^{D1} and E_{ML}^{D2} .  [The period "." is not part of the equation.] By means of Eqs.(19) and (21) these values are transformed into the static modulus of elasticity (E_{ST-MH}^D ,  [The comma "," is not part of the equation.] E_{ST-ML}^{D1} and E_{ST-ML}^{D2}). In the homogeneous model, E_{ST-MH}^D is the global static modulus obtained from modal analysis, which can be directly compared with the experimental modulus E_{ST}^D .  [The period "." is not part of the equation.] However, in the substructured models, the two moduli of each lamella are used to simulate the standardized four-point bending test, using Eq. (2) to obtain the global E_{G-ML}^D ,  [The comma "," is not part of the equation.]

equation.] which can be compared with the static modulus E_{ST}^D . [The period "." is not part of the equation.] The errors in the estimation of the static modulus of elasticity are evaluated by,

$$\varepsilon_{Meth}^D \left(\% \right) = \left| \frac{E_{G-Meth}^D - E_{ST}^D}{E_{ST}^D} \right| 100$$

where ε_{Meth}^D is the error in the estimation of the equivalent static elasticity modulus (E_{G-Meth}^D) from ultrasound testing ($Meth = US$), modal update in homogeneous model ($Meth = MH$), or modal update in substructured model ($Meth = ML$). This equation compares these estimations with respect to the static modulus, E_{ST}^D , [The comma "," is not part of the equation.] obtained from the standardized bending test.

2.7. Statistical and regression analysis

Correlation analysis between variables was performed using simple linear regression and multiple regression analysis. Nonlinear models were not considered because all models fit well into linear correlations. The regression model is formulated according to the following equation,

$$y = A_i + B_i x_1 + C_i x_2 + \varepsilon$$

where y is the response, A_i is the intercept and B_i and C_i are the constant coefficients or slopes in the model, x_1 and x_2 are the observations or predictors, and ε is the error. In univariate models, the coefficient $C = 0$.

The statistical differences between variables were assessed using the coefficient of determination R^2 . Hypothesis testing was used to verify the independence of the means when comparing results from the same type of test. The analysis of the variance (ANOVA) test was conducted to verify the existence of the regression. The null hypothesis means that the predictors do not provide any information about the response, while the alternative hypothesis checks the existence of the linear relationship between predictors and the response. The analysis of the covariance (ANCOVA) was used to compare two regression lines to each other. This analysis compares the slopes and the intercepts and determine whether they belong to the same or different groups. ANCOVA makes the assumptions of linear regression with normality and homoscedasticity.

Significant differences were accepted when $p < 0.05$.

3. Results

A summary of the moisture content (MC) and the static modulus of elasticity obtained for the different types of samples in the experimental survey are shown in Table 2. On average, the MOE obtained by ultrasound measurements in the longitudinal direction is higher than the static MOE (mean difference 55.8% and SD = 1.10), whereas the MOE obtained by modal updating is slightly lower (mean difference value −2.8% and SD = 0.79). These values are in agreement with the results provided by other authors (Fernández-Serrano and Villasante 2021; Hassan, Horáček, and Tippner 2013). In the next sections, the detailed results obtained for the MOEs in the three steps are presented.

Note: The table layout displayed in ‘Edit’ view is not how it will appear in the printed/pdf version. This html display is to enable content corrections to the table. To preview the printed/pdf presentation of the table, please view the ‘PDF’ tab.

Table 2. Overall statistical results of the moisture content and static modulus of elasticity obtained according to European Standard EN 408:2010. [+](#)

Type	Species	MC (%)		E _{ST} (MPa)	
		Mean (SD)	Max.–Min.	Mean (SD)	Max.–Min.
Simple	Pinus S.	15.4 (0.37)	16.0–14.9	8512.1 (2825.41)	14079.2–4638.5
	Spruce	15.7 (0.70)	17.7–15.0	10478.5 (2105.45)	14702.4–6939.9
Duo	Pinus S.	16.8 (1.32)	17.2–15.0	9758.1 (644.27)	10674.6–8719.2
	Spruce	15.5 (0.28)	15.9–15.0	7946.8 (872.14)	9119.3–6972.5
Glulam	Pinus S.	16.5 (0.84)	17.7–15.4	7418.8 (871.33)	8034.9–6802.7
	Spruce	14.86 (0.28)	15.2–14.6	8491.6 (251.72)	8669.6–8313.6

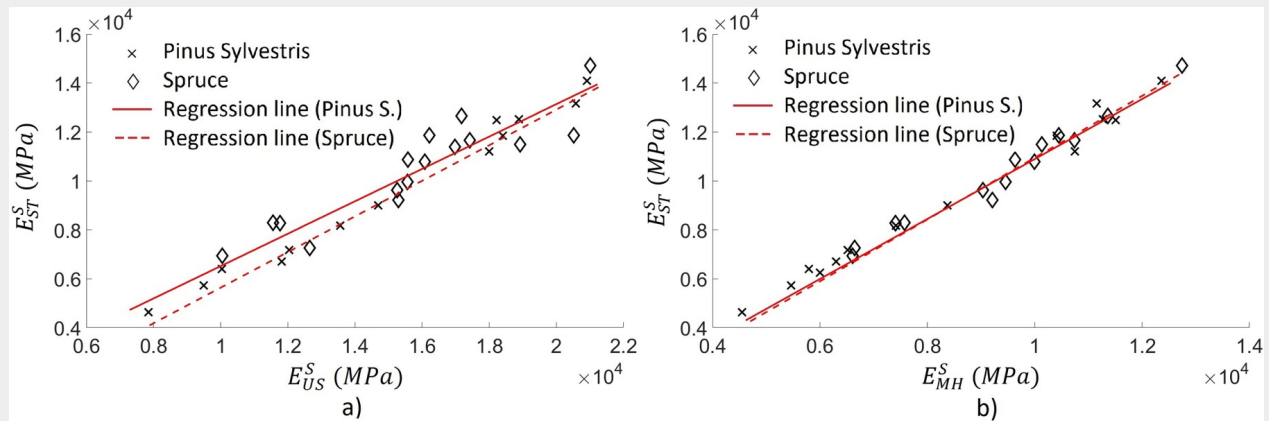
Place the cursor position on table column and click 'Add New' to add table footnote.

3.1 Results in step 1: single beams

The first issue considered in the comparison of the MOEs is whether the results of one species could be grouped together with the other one; otherwise, they should be treated separately. To this end, the analysis of

covariance (ANCOVA) was performed by comparing the regression lines of each species. The first null hypothesis compares the slope of both lines. If this hypothesis is accepted the slopes of both lines are considered equal (i.e., parallel lines). The second null hypothesis considers that both regression lines intercept the coordinate axes at the same point. The acceptance of the two null hypotheses means that both lines are the same line and the two species can be treated as only one group. Figure 11(a) shows the two linear models for each species in the comparison of E_{ST}^S vs. E_{US}^S , [The comma "," is not part of the equation.] and Fig. 11(b) shows the same comparison for E_{ST}^S vs. E_{MH}^S . [The period "." is not part of the equation.] It can be observed that in both cases the lines for the two species are quite similar; however, it is necessary to demonstrate statistically that they are the same line. The analysis of the covariance in the relationship between E_{ST}^S and E_{US}^S demonstrates that the slope and the intercept of the two lines are the same because the p -value is greater than the 5% of the significance level ($p = 0.789$). The covariance analysis for the comparison of E_{ST}^S and E_{MH}^S also confirms this hypothesis ($p = 0.502$) and, therefore, both species can be analyzed together.

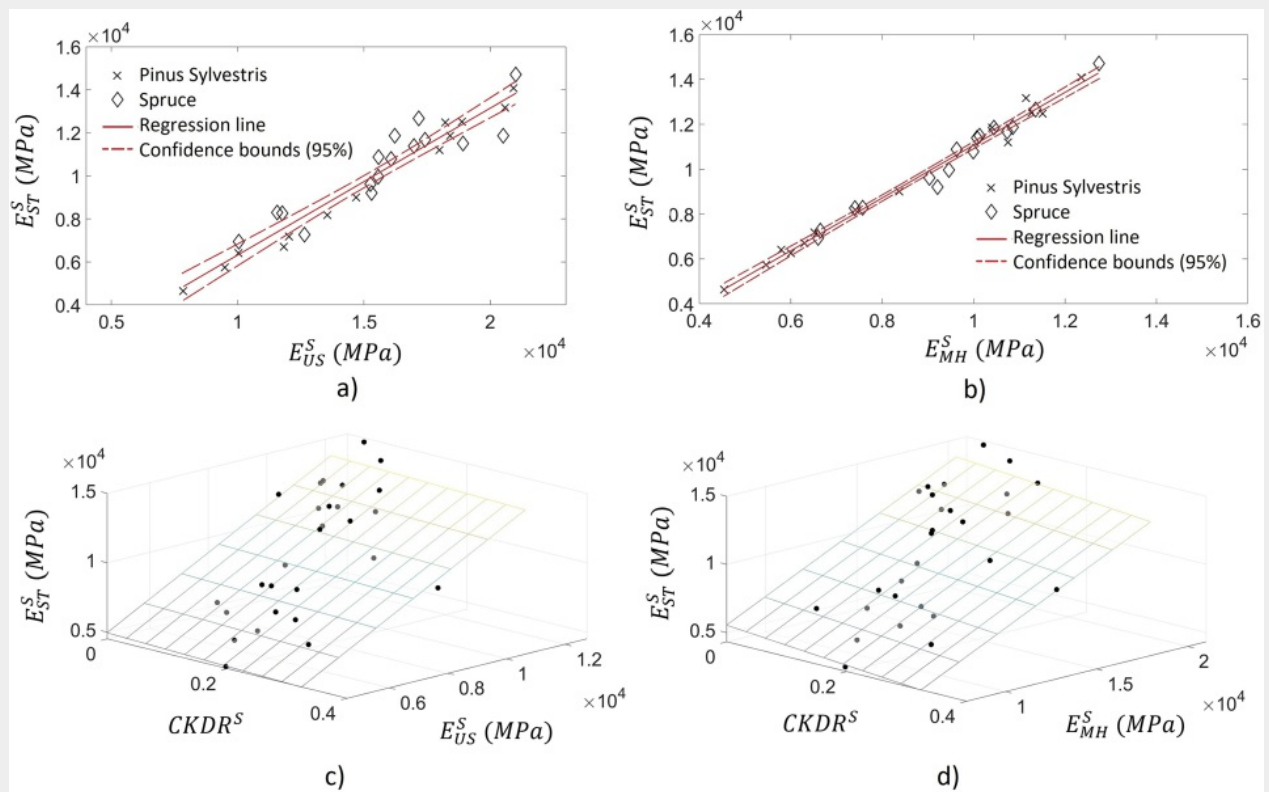
Figure 11. Linear regressions for Spruce and Pinus Sylvestris species in the comparison of (a) E_{ST}^S vs. E_{US}^S and (b) E_{ST}^S vs. E_{MH}^S +



Figures 12(a) and 12(b) show the results of the bivariate regression analysis of the two species grouped together. These models provide the static modulus of elasticity (i.e., E_{ST}^S) from the modulus obtained from ultrasound measurements (i.e., E_{US}^S), and modal analysis (i.e., E_{MH}^S), respectively. In these figures, the solid lines provide the linear models and the dashed lines establish the confidence bounds of 95%. Table 3 shows the parameters of the regression lines for the two traces (models 1 and 2). The analysis of the variance test (ANOVA) was performed to check the validity of the regression models. The values of R^2 and p are shown in this table. In the two models, R^2 is higher than 0.9 and the p -value was found less than 0.05 (i.e., 5%), reflecting the good correlation between MOEs. However, the R^2 value for the relationship of $E_{ST}^S - E_{US}^S$ is

lower than for $E_{ST}^S - E_{MH}^S$. [The period "." is not part of the equation.] Despite the good correlation, a bivariate correlation model was studied to ascertain the influence of knots on the predictions. For this reason, the Concentrated Knot Diameter Ratio ($CKDR$) was included as the second predictor and the results are shown in Figs. 12(c) and 12(d). The statistical parameters are shown in Table 3 (models 3 and 4). In the case of $E_{ST}^S - E_{US}^S$ there is a clear influence of the $CKDR$ ($C_3 = -3181.1$) with an improvement in R^2 with respect to the bivariate regression model. However, the influence of the $CKDR$ on the $E_{ST}^S - E_{MH}^S$ relationship is less ($C_4 = -1027.5$) and R^2 does not undergo a significant variation.

[In the Figure 12 caption, the comma "," after Est^s, and the comma "," after Eus^s are not part of the equation.] Figure 12. Linear regression between E_{ST}^S , E_{US}^S , and E_{MH}^S in single beams for the two timber species: (a) model for ultrasound tests, (b) model for homogeneous modal updating, (c) influence of the $CKDR$ in ultrasound tests, and (d) in modal tests. +




Note: The table layout displayed in 'Edit' view is not how it will appear in the printed/pdf version. This html display is to enable content corrections to the table. To preview the printed/pdf presentation of the table, please view the 'PDF' tab.

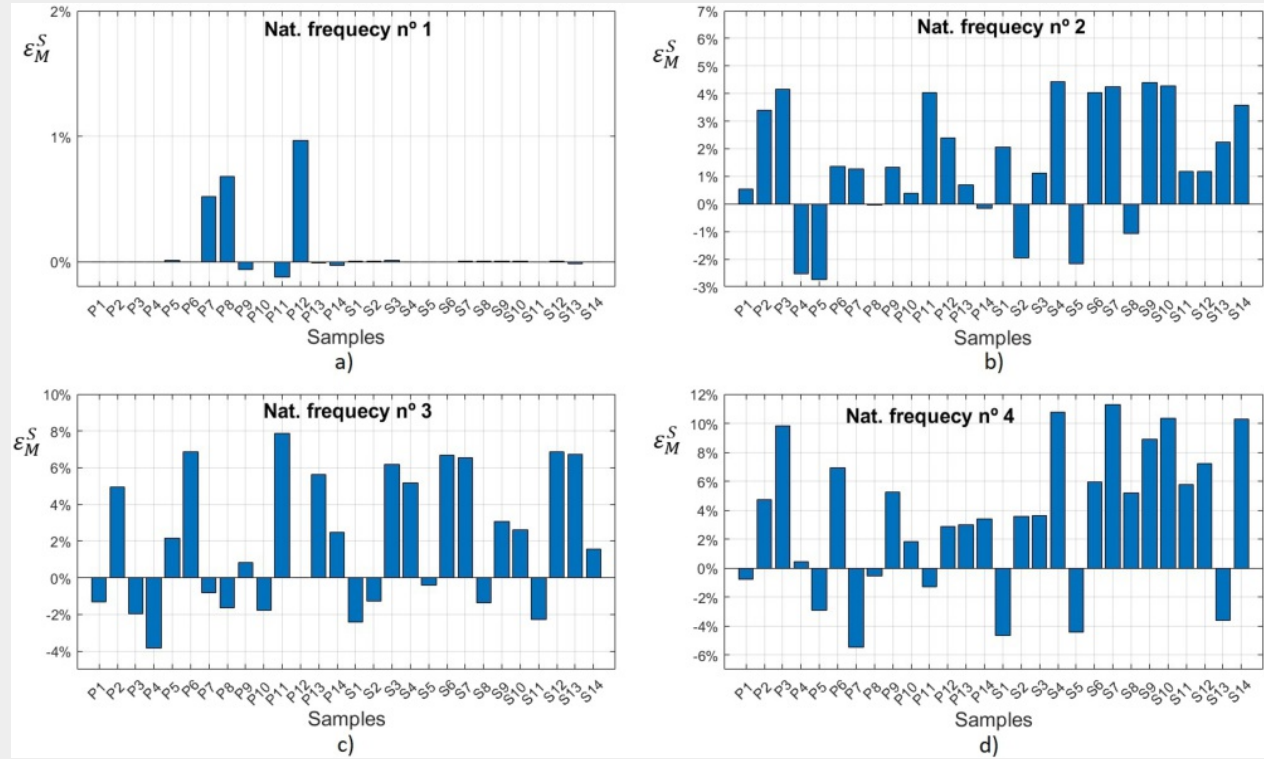
Table 3. Parameters and statistics in the models of linear regression for single beams. +

Relationship	Models	<i>A</i>	<i>B</i>	<i>C</i>	R^2	<i>p</i> -vaule
$E_{ST}^S - E_{US}^S$	1	-515.7	0.6785	–	0.925	<0.05
$E_{ST}^S - E_{MH}^S$	2	-673.1	1.1732	–	0.982	<0.05
$E_{ST}^S - E_{US}^S - CKDR^S$	3	421.4	0.6	-3181.1	0.937	<0.05
$E_{ST}^S - E_{HM}^S - CKDR^S$	4	-364.3	1.2	-1027.5	0.982	<0.05

Place the cursor position on table column and click 'Add New' to add table footnote.

The comparison of the natural frequencies obtained from experimental tests and the numerical model (FEM_H^S) is shown in Fig. 13. This figure shows the errors obtained by using Eq. (17) in the first four natural frequencies for the Pinus Sylvestris (P1-14) and Spruce (S1-14) species. For the first natural frequencies, the mean value of the error is 0.07% (SD = 0.239%). The mean value of the errors for the second, third and fourth natural frequencies are increasing, and they are 1.49% (SD = 2.247%), 2.04% (SD = 3.677%), and 3.47% (SD = 5.060%), respectively. This increment in errors is a common effect in modal analysis because the imperfections of the material and boundary conditions have a greater influence in higher modes (Altunışık, Okur, and Kahya 2017).

Figure 13. Errors obtained in the theoretical determination of the natural frequencies in modal analysis using the model FEM^S_H for Pinus Sylvestris and Spruce species: (a) first mode, (b) second mode, (c) third mode, and (d) fourth mode. 



3.2. Results in step 2: duo-laminated beams

Following the process established in Fig. 10, the static modulus of elasticity (E_{ST}^D) was obtained by using the standardized test for the 17 duo-laminated beams. On the other hand, using the MC corrections (European Standard EN 384:2016 + A1 2010), given by the direct ultrasound measurements were transformed in the modulus of elasticity in the two lamellas of each specimen (i.e., E_{US}^{D1} and E_{US}^{D2}). These moduli are converted into the equivalent static modulus (E_{ST-US}^D) using the two aforementioned models, which are reformulated here by substituting the constants with their values (see Table 3) as follows.

$$E_{ST-US}^{Di} = -515 + 0.6785 E_{US}^{Di}$$

$$E_{ST-US(CKDR)}^{Di} = 421.4 + 0.600 E_{US}^{Di} - 3181.1 CKDR^{Di}$$

The first equation provides the equivalent static modulus of elasticity for each lamella given by the regression model without considering the influence of the knots. Equation (25) provides the same value but includes the influence of the *CKDR* in the estimation.

These static moduli of elasticity are used to simulate the standardized static bending test using the finite element model FEM_L^D . [The period "." is not part of the equation.] By using Eq. (2), this simulation provides the global static modulus of each double beam (i.e., E_{G-US}^D). In Fig. 14 this modulus is compared with the static modulus obtained from the experimental tests. Table 4 shows the constants and statistical parameters of the regression lines (models 5 and 6). The coefficient of determination (R^2) is higher when *CKDR* is considered. Furthermore, the ANCOVA analysis determines that the two regression lines (with and without the influence of *CKDR*) are not the same ($p < 0.05$). Fig. 15 shows the errors using Eq. (22) for the 17 samples (D1-D17) in the estimation of static modulus of elasticity from ultrasound measurements. The results without considering the *CKDR* are blue bars whereas the red ones include the *CKDR* in the estimation. Excepting one case with a very low concentration of knots (sample D15), the consideration of the *CKDR* produces an important reduction in the errors and, consequently, an improvement in the estimation of the E_{ST}^D . [The period "." is not part of the equation.] In fact, the mean error without *CKDR* is 15.1% (SD = 5.03%), whereas the mean error considering the effect of *CKDR* is 7.0% (SD = 3.40%). This difference is significant (ANOVA test, $p < 0.05$).

Figure 14. Linear models for the correlation between the E_{ST}^D and E_{G-US}^D with and without considering the influence of the *CKDR*. [+](#)

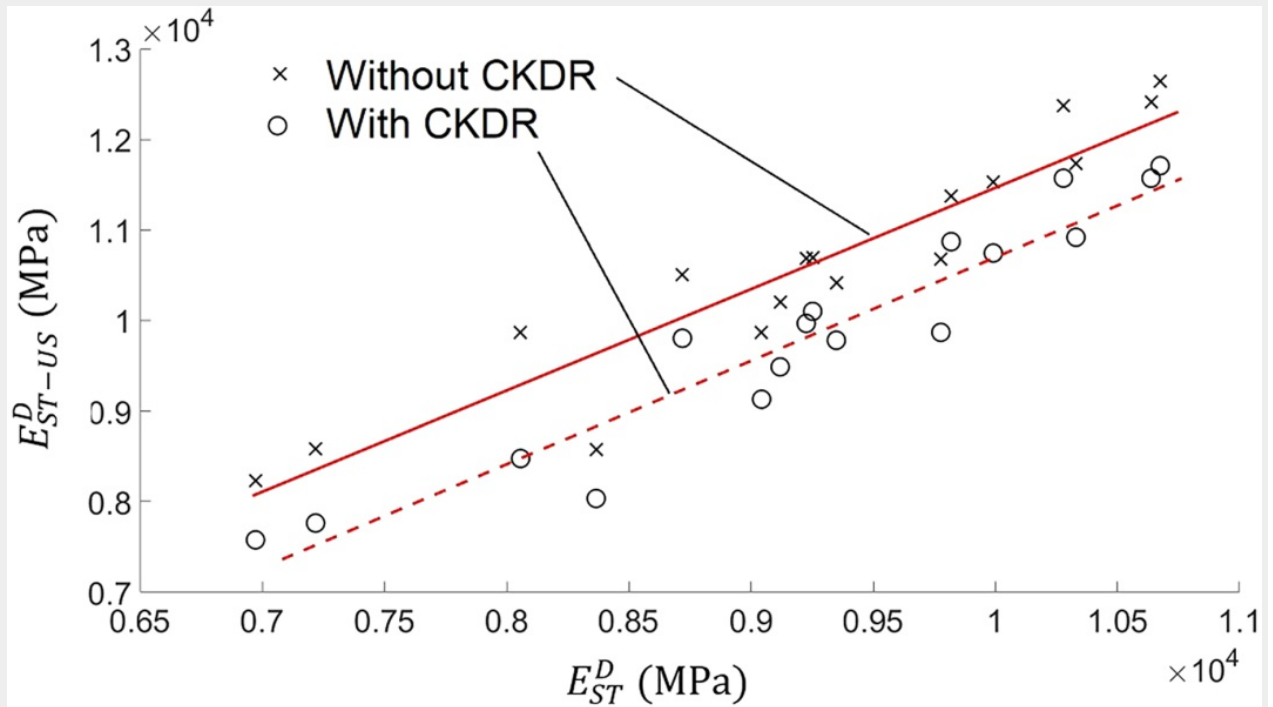
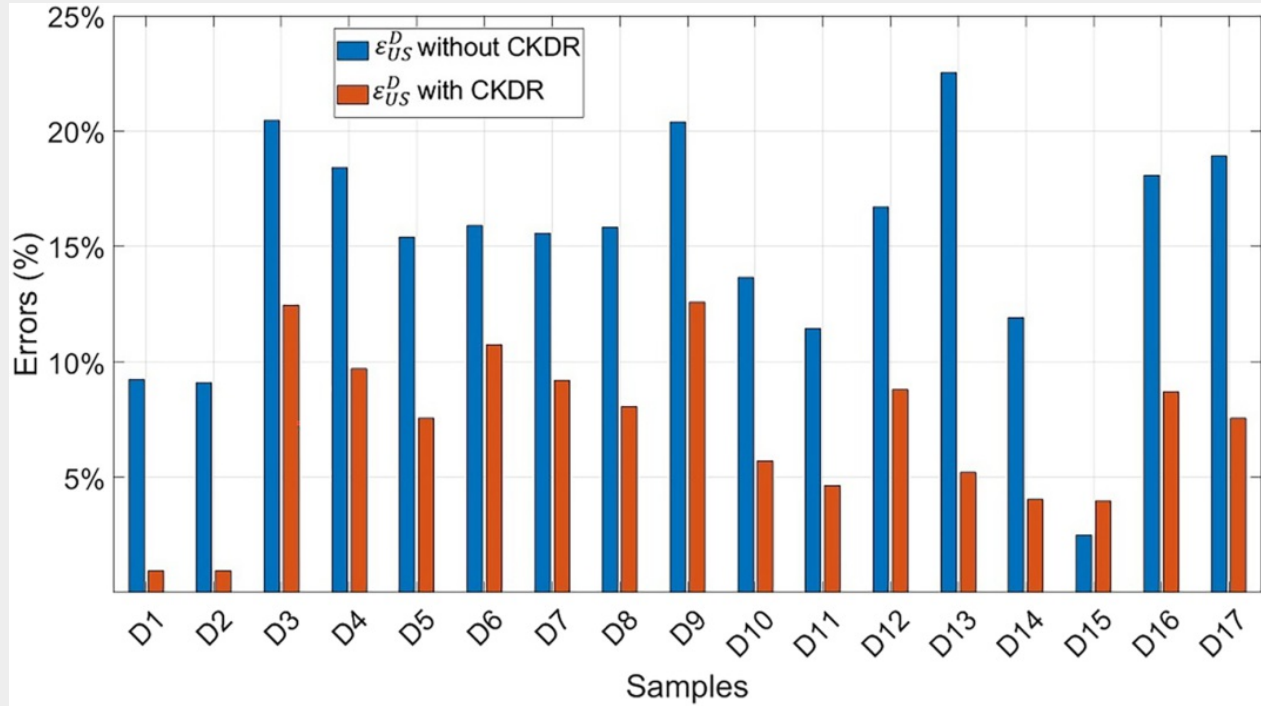


Figure 15. Errors in the estimation of the static modulus of elasticity from the ultrasound measurements with and without considering the influence of the *CKDR*. [+](#)



Note: The table layout displayed in ‘Edit’ view is not how it will appear in the printed/pdf version. This html display is to enable content corrections to the table. To preview the printed/pdf presentation of the table, please view the ‘PDF’ tab.

Table 4. Comparison of the static modulus of elasticity and the equivalent values obtained from ultrasound and modal updating in duo-laminated beams. [+](#)

Relationship	Models	A	B	R^2	p -vaule
$E_{ST}^D - E_{G-US}^D$	5	16.427	1.14850	0.890	<0.05
$E_{ST}^D - E_{G-US}^D - CKDR^D$	6	-771.710	1.15100	0.914	<0.05
$E_{ST}^D - E_{ST-MH}^D$	7	4658.600	0.49299	0.376	<0.05
$E_{ST}^D - E_{ST-MH}^D - CKDR^D$	8	4629.100	0.49604	0.334	<0.05

$E_{ST}^D - E_{G-ML}^D$	9	-372.710	1.01640	0.937	<0.05
$E_{ST}^D - E_{G-ML}^D - CKDR^D$	10	-467.210	1.04900	0.940	<0.05

Place the cursor position on table column and click 'Add New' to add table footnote.

Figure 16 shows the results in the determination of the static modulus of elasticity from the updating dynamic models, FEM_H^D and FEM_L^D . [The period "." is not part of the equation.] When the homogeneous model is used, the R^2 coefficients are very low (Table 4, model 7 and 8) regardless of the consideration of the CKDR (see Fig. 16a). However, the substructured finite element model (see Fig. 16b) provides a good estimation of the static modulus of elasticity. Indeed, the dispersion of the results is lower, and this fact is reflected in the higher values of R^2 coefficients in both models, without CKDR (Table 4, model 9) and with CKDR (Table 4, model 10). Figure 17 shows the errors in the four models. For the homogeneous model without CKDR (model 7) the mean error is 7.2% (SD = 6.98%), while considering CKDR (model 8) provides a mean error of 7.6% (SD = 6.89%). This difference is not significant (ANOVA test, $p = 0.991$). The substructured model without CKDR (model 9) has a mean error of 3.2% (SD = 2.37%), and with CKDR (model 10) the mean error is 2.76% (SD = 1.57%). However, this difference is not significant (p -value = 0.051).

Figure 16. Estimation of static modulus of elasticity using modal analysis with and without CKDR influence in: (a) homogeneous models (FEM_H^D), and (b) substructured models (FEM_L^D). +

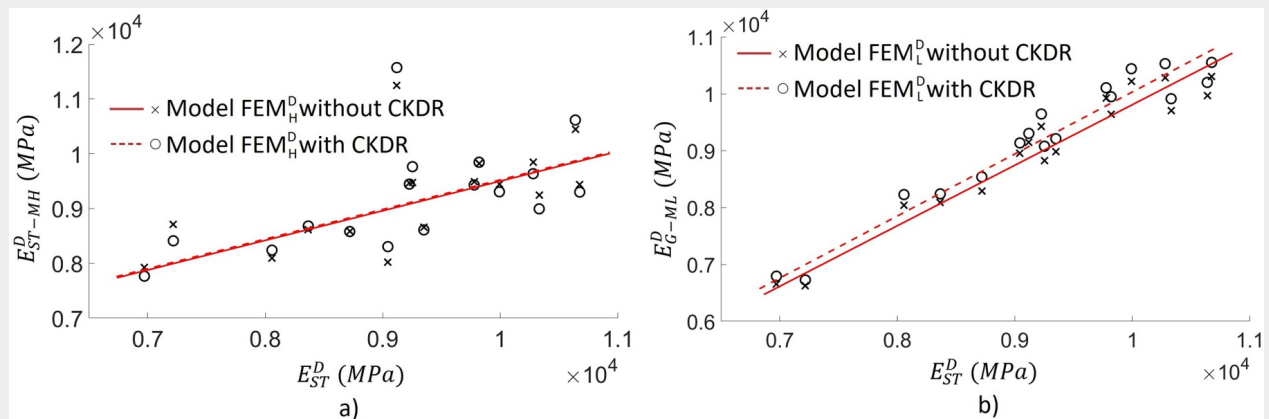
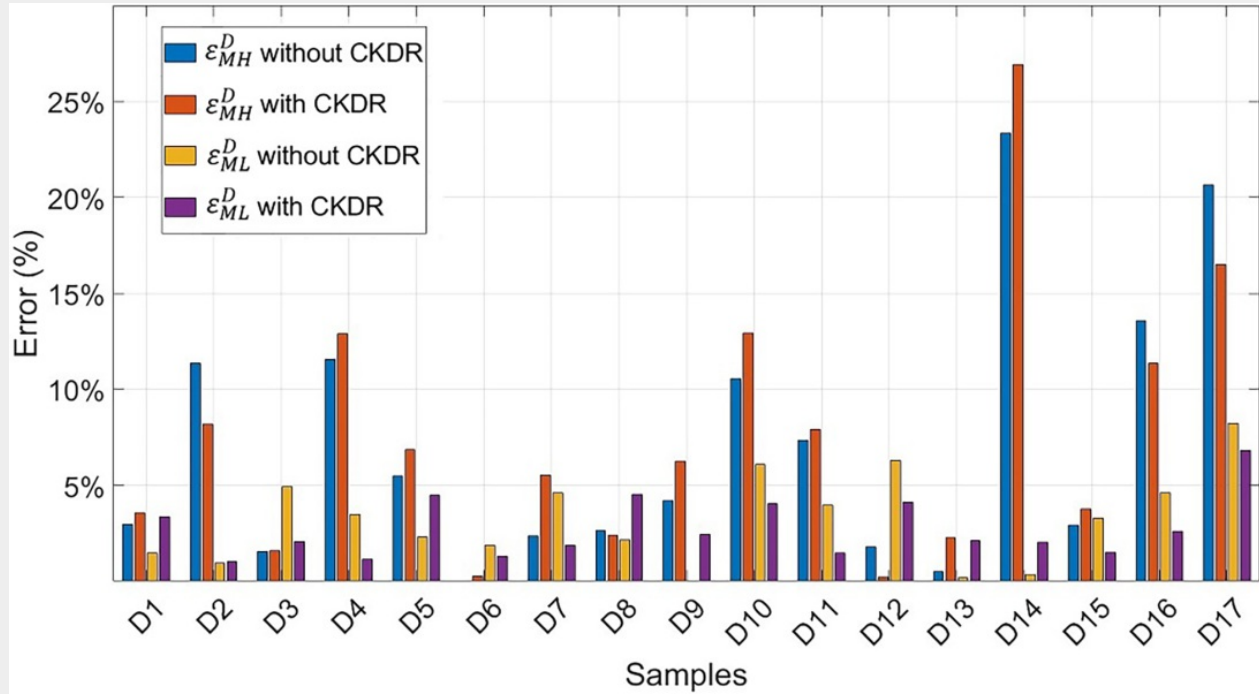


Figure 17. Errors in the estimation of the static modulus of elasticity (i.e., E_{ST-MH}^D and E_{G-ML}^D) from modal analysis using homogeneous and substructured models. [+](#)




3.3. Results in step 3: glulam beams

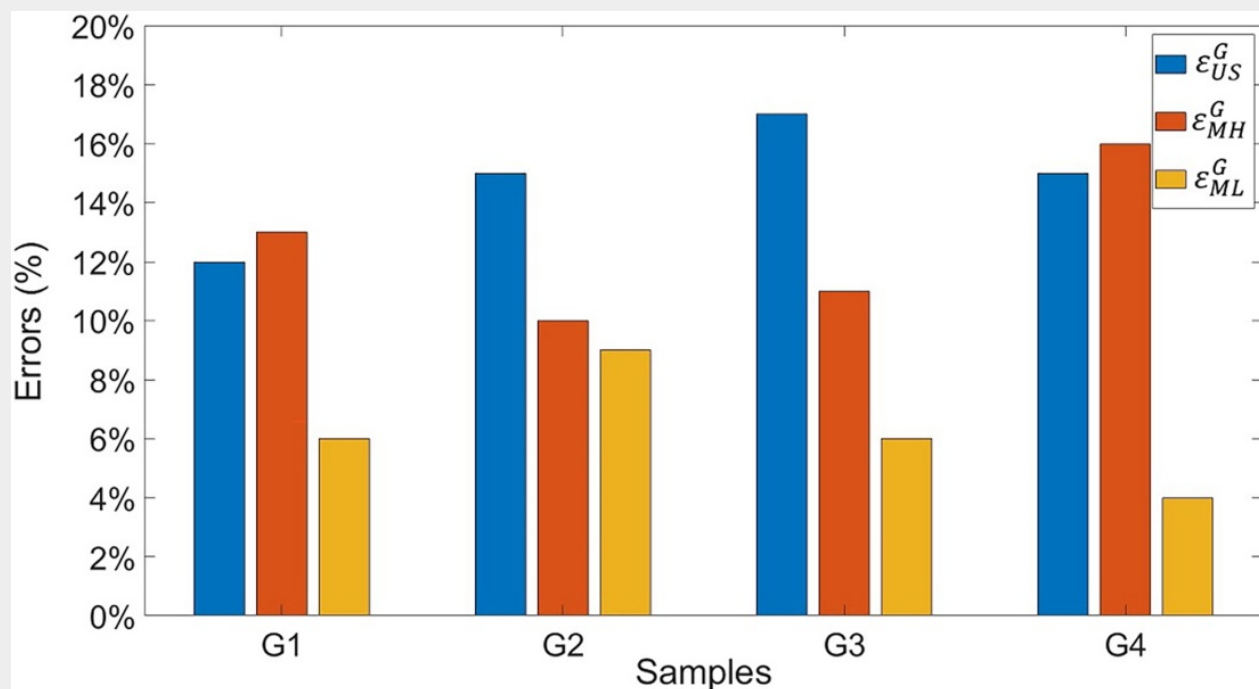
The four specimens of glulam beams were submitted to the same process as duo-laminated beams. However, since the glulam beams were assembled prior to this study, it was not possible to evaluate the knot concentration in the lumber surfaces to determine the *CKDR*. Thus, all the analyses were carried out without considering the *CKDR*. Although this seems an awkward assumption in this work, this situation is similar to reality when an actual NDT is performed.

The standardized bending four-point test was used to obtain the static modulus of elasticity, E_{ST}^G , [The comma "," is not part of the equation.] of the beams. Ultrasound measurements provided the modulus of elasticity (E_{US}^{Gi}) in the four lamellas of each beam. The equivalent static modulus of elasticity (E_{ST-US}^{Gi}) was obtained by means of using model 1 given in Table 3. After that, these moduli were used to model the stiffness of each substructure in FEM_L^G and simulate the static four-point bending test to obtain the global static modulus of elasticity in each specimen, i.e., E_{G-US}^G . [The full stop "." is not part of the equation.]

Modal updating was carried out using experimental data from modal analysis. This analysis enabled the

dynamic modulus of elasticity to be obtained in the homogenous finite element model (FEM_H^G) and in the substructured one (FEM_L^G). In the former, the local search optimization approach provided the E_{MH}^G [The comma "," is not part of the equation.] which was introduced in model 2 (see Table 3) to obtain the E_{ST-MH}^G [The period "." is not part of the equation.] On the other hand, the PSO algorithm was used to update the substructured model FEM_L^G [The comma "," is not part of the equation.] obtaining E_{ML}^{Gi} in each lamella, which was used in model 2 to obtain the equivalent static modulus E_{ST-ML}^{Gi} [The period "." is not part of the equation.] These moduli were used to simulate the static bending test in the finite element model, obtaining the global modulus of elasticity E_{G-ML}^G [The period "." is not part of the equation.] Table 5 shows the comparison of the E_{ST}^G [The comma "," is not part of the equation.] E_{G-US}^G [The comma "," is not part of the equation.] E_{ST-MH}^G [The comma "," is not part of the equation.] and E_{G-ML}^G [The period "." is not part of the equation.] Figure 18 shows the errors in the comparison of the estimated static modulus with respect to the one obtained from the standardized test. The mean error for ultrasound is 14.4% (SD = 2.25%), for modal updating in the homogeneous model it is 12.2% (SD = 2.55%), and for the non-homogeneous model 6.3% (SD = 1.86%). The differences between errors in each kind of test are significant (ANOVA test, $p < 0.05$).

Figure 18. Errors in the estimation of the static modulus of elasticity obtained from ultrasound (E_{G-US}^G), modal analysis in homogeneous (E_{ST-MH}^G) and non-homogeneous (E_{G-ML}^G) glulam beams. 



Note: The table layout displayed in 'Edit' view is not how it will appear in the printed/pdf version. This html display is to enable content corrections to the table. To preview the printed/pdf presentation of the table, please view the 'PDF' tab.

Table 5. Static modulus of elasticity obtained from the standardized test and those obtained from ultrasound tests and modal analysis. +

Specimen	Species	E_{ST}^G	E_{G-US}^G	E_{ST-MH}^G	E_{G-ML}^G
G1	Pinus S.	6802.68	7586.21	5946.81	7203.14
G2	Pinus S.	8034.93	9205.23	7240.51	7335.94
G3	Spruce	8669.58	10144.45	7744.40	8112.04
G4	Spruce	8313.59	9538.73	7016.13	7965.57

Place the cursor position on table column and click 'Add New' to add table footnote.

4. Discussion

This work analyzed whether the ultrasound measurements and modal updating are accurate NDT techniques for estimating the bending modulus of elasticity in glulam elements. The study is not focused on the detection of a specific kind of damage, but on the assessment of the accuracy in the estimation of the MOE. In fact, the structural elements tested are healthy beams with a broad range of stiffness. The results provide the errors in the evaluation of MOE under controlled laboratory conditions. In this way, the results obtained could be extrapolated to onsite NDT inspection of glulam.

To this end, three kinds of beam specimens were tested. Single beams were used to obtain the basic features of the material. The results from these specimens showed that the two species (i.e., *Pinus Sylvestris* and Spruce) can be grouped together to estimate the MOE from NDT results. This is because the two correlation models do not show significant differences. The results of the experimental tests show the influence of knots in the MOE estimation. In fact, knots produce a gradual decrease in the static and dynamic MOEs. This influence of knots in the estimation of MOE is implemented in this work by means of the *CKDR* as a predictor in the bivariate models. The results show that knots increase the uncertainty in ultrasound measurements. Indeed, the correlation without the *CKDR* between the E_{US}^s and E_{ST}^s is $R^2 = 0.925$ and considering the *CKDR* it is incremented to $R^2 = 0.937$. In modal updating, this influence is much smaller and there is no change in the


correlation coefficient. Furthermore, the correlation between static and modal MOEs is greater than the correlation obtained between static and ultrasound MOEs ($R^2 = 0.937$ in the ultrasound approach vs. $R^2 = 0.982$ in modal updating). Ultrasound techniques for MOE estimation are more sensitive to the presence of knots or clustered knots than modal updating. The explanation for this effect can be found in uncertainties produced by alterations due to knots in wave propagation. Despite this drawback, the results of ultrasound measurements in single beams can be considered good enough since the correlation is higher than 0.9 in all cases.

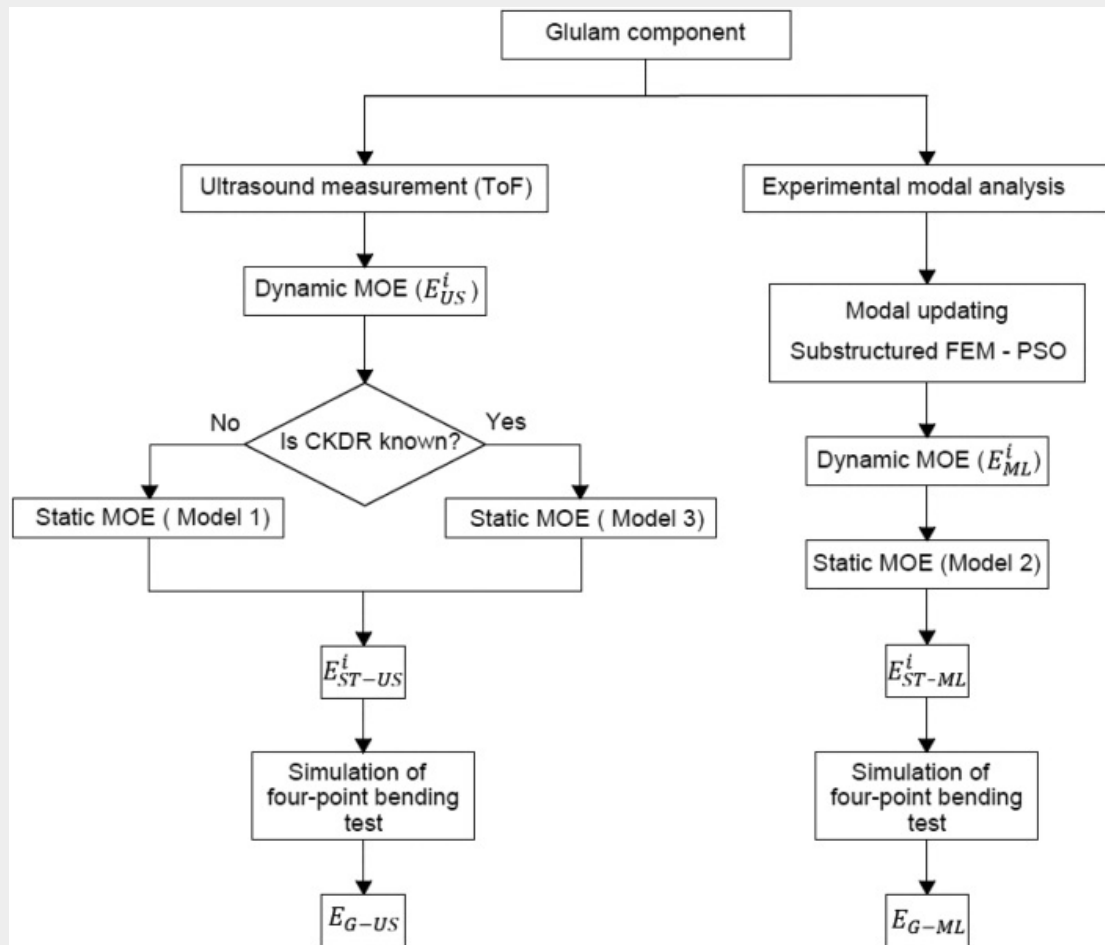
In duo-laminated beams, the estimation of the static MOE by means of ultrasound measurements shows significant differences between the univariate and bivariate models. This fact highlights the influence of the presence of knots in the assessment of the stiffness, and how the consideration of the *CKDR* improves this estimation. Modal updating in duo-laminated beams shows that the consideration of substructures provides greater accuracy in estimating the modulus of elasticity. Indeed, a very low coefficient of determination is obtained in the relation between MOEs for homogeneous models, but substructured models strongly improve the results. It is important to point out that small differences in the dynamic modulus in each lamella provide important changes in natural frequencies and mode shapes. Thus, the adjustment of the dynamic MOE is strongly influenced by these variations. Although lower errors have been obtained when the *CKDR* was considered in the MOE estimation, the differences found are not significant. Thus, it can be concluded that the use of the *CKDR* has a negligible influence on modal updating. The different influences that the presence of knots produces in the two approaches when estimating the elastic modulus should be noted. While ultrasound-based measurements are strongly influenced by *CKDR*, the modal update method is not. This effect can be explained because in modal analysis the reduction of bending stiffness produced by knots is implicit in the results obtained from experiments in the natural frequencies and mode shapes. However, in acoustic methods, the presence of knots distorts the propagation of waves, generating random effects which are not directly related to the stiffness.

In the glulam specimen tests, the errors show the same trend as in simple and duo-laminated specimens, that is, the maximum error is obtained with the ultrasound-based approach (17.0%), although, in some individual cases the homogeneous model produces the maximum error. In all cases, the best results are obtained for modal updating with the non-homogeneous model (min. error = 4.2% - max. error = 8.7%).

The level of confidence of the results shows that neither the ultrasound-based approach nor modal updating achieve the necessary accuracy to work alone as an NDT technique on large structures of glulam timber. The acoustic measurement is influenced by the presence of knots, and their concentration cannot be accurately determined by inspection. Thus, a variability of the results can be expected in the assessment in-situ. On the other hand, the modal updating approach provided a reasonable level of accuracy. However, the experimental modal analysis performed in this work was carried out in the laboratory under controlled conditions. Actual glulam structures are much more complex and additional uncertainties could be expected caused by the variation in geometry, boundaries, defects, etc (Zhai et al. 2023). Thus, further experimental tests should be performed in laboratory and in-situ to explore the capabilities and limitations of the proposed approaches.

Finally, based on everything discussed above, the two most suitable procedures for predicting the static modulus of elasticity using ultrasound measurements and modal updating are established. These procedures are shown in Fig. 19, outlining the steps to be followed in each case. In the case of ultrasound, the dynamic MOE is first obtained using Eq. (3) and, if the CKDR is unknown, Model 1 from Table 3 is used to estimate the static MOE for each lamella. If the CKDR for all specimens were known, the static modulus would be estimated using Model 3. Once the static MOE of each specimen is obtained, the overall static MOE of the component is determined through finite element simulation.

Figure 19. Proposed methodology for the determination of static MOE using ultrasound techniques and modal updating. 



On the other hand, modal updating starts with experimental modal analysis, providing the natural frequencies and mode shapes of the actual system. These data, together with the substructured numerical models and the

PSO approach, enable the determination of the dynamic MOE of each lamella. Subsequently, the prediction of the static modulus for each lamella is obtained using Model 2 from [Table 3](#). Once these values are established, they are incorporated into the finite element model to obtain the global static MOE.

These procedures enable the static MOE of structural systems in service to be obtained and compared with the static MOE of the healthy structure. The differences indicate whether there has been a reduction in the structural capacity and if any type of repair is required.

5. Conclusions

The results of this study demonstrate that ultrasound and modal updating techniques serve as good predictors for the static bending modulus of elasticity in glulam elements. However, it should be noted that the ultrasound technique tends to overestimate the static modulus, while the modal-updating approach underestimates it. Nevertheless, the strong correlation found among the MOEs demonstrates the validity of the linear models for prediction. Based on the experimental analysis and numerical simulations carried out in this study, the following conclusions can be drawn:

1. The predictions made with the models do not exhibit significant differences when either *Pinus sylvestris* or spruce species are used. Thus, the linear models obtained from the experimental analysis can be used for both species without modifying the slope or intercept coefficients.
2. The density and concentration of knots have a significant influence on the estimation of the static modulus of elasticity when employing the ultrasound technique. Whenever the CKDR is available, it should be included in the estimation of the static modulus using model 3 ([Table 3](#)). Otherwise, model 1 (also presented in the same table) could be used, albeit with a slight decrease in accuracy while maintaining reasonable precision.
3. Modal updating requires the use of substructures to model the lack of homogeneity in glulam elements. The use of homogeneous models resulted in outcomes with a large dispersion and poor accuracy. The distinct elasticity properties in each lamella give rise to changes in natural frequencies and mode shapes that can be obtained through optimization. The PSO-based algorithm demonstrates good accuracy in determining these changes.
4. The consideration of the CKDR in the modal updating approach has a negligible influence on the results. The influence of knot density and its concentrations is implicitly captured in the outcomes provided by modal analysis, given the accurate estimation of the static MOE. Thus, model 2 in [Table 3](#) yields the best results for obtaining the static modulus in each lamella.

5. Both methods provide a reliable estimation of the static modulus of elasticity. However, the modal update approach proves to be more reliable than the ultrasound-based technique under laboratory conditions. Despite the good accuracy achieved in the predictions from this study, it is important to emphasize that the on-site application of these assessment techniques requires the incorporation of more realistic boundary conditions in the experimental tests.




Disclosure statement

The authors report there are no competing interests to declare.




Note: this Edit/html view does not display references as per your journal style. There is no need to correct this. The content is correct and it will be converted to your journal style in the published version.

References




- Alkayem, N. F., M. Cao, and M. Ragulskis. 2019. Damage Localization in Irregular Shape Structures Using Intelligent FE Model Updating Approach with a New Hybrid Objective Function and Social Swarm Algorithm. *Applied Soft Computing* 83:105604. doi:10.1016/j.asoc.2019.105604. [AQ2](#)   
- Altunışık, A. C., F. Y. Okur, and V. Kahya. 2017. Modal Parameter Identification and Vibration Based Damage Detection of a Multiple Cracked Cantilever Beam. *Engineering Failure Analysis* 79:154–70. doi:10.1016/j.engfailanal.2017.04.026.   
- Altunışık, A. C., F. Y. Okur, S. Karaca, and V. Kahya. 2019. Vibration-Based Damage Detection in Beam Structures with Multiple Cracks: Modal Curvature vs. Modal Flexibility Methods. *Nondestructive Testing and Evaluation* 34 (1):33–53. doi:10.1080/10589759.2018.1518445.   
- Arriaga, F., C. Osuna-Sequera, I. Bobadilla, and M. Esteban. 2022. Prediction of the Mechanical Properties of Timber Members in Existing Structures Using the Dynamic Modulus of Elasticity and Visual Grading Parameters. *Construction and Building Materials* 322:126512. doi:10.1016/j.conbuildmat.2022.126512.   
- Barroso, L. R., and R. Rodriguez. 2004. Damage Detection Utilizing the Damage Index Method to a Benchmark Structure. *Journal of Engineering Mechanics* 130 (2):142–51. doi:10.1061/(asce)0733-9399(2004)130:2(142).   
- Bucur, V. 2006. *Acoustics of Wood*. Berlin Heidelberg: Springer.   
- Cavalli, A., L. Bevilacqua, G. Capecchi, D. Cibecchini, M. Fioravanti, G. Goli, M. Togni, and L. Uzielli.

2016. MOE and MOR Assessment of in Service and Dismantled Old Structural Timber. *Engineering Structures* 125:294–9. doi:10.1016/j.engstruct.2016.06.054.   

Chen, H., and S. Li. 2022. Collinear Nonlinear Mixed-Frequency Ultrasound with FEM and Experimental Method for Structural Health Prognosis. *Processes* 10 (4):656. doi:10.3390/pr10040656.   


Cuadrado, J., M. Zubizarreta, B. Pelaz, and I. Marcos. 2015. Methodology to Assess the Environmental Sustainability of Timber Structures. *Construction and Building Materials* 86:149–58. doi:10.1016/j.conbuildmat.2015.03.109.   


Divós, F., and T. Tanaka. 2005. Relation Between Static and Dynamic Modulus of Elasticity of Wood. *Acta Silvatica et Lignaria Hungarica* 1 (January 2005):105–10.   

Doebling, S. W., C. R. Farrar, and M. B. Prime. 1998. A Summary Review of Vibration-Based Damage Identification Methods. *The Shock and Vibration Digest* 30 (2):91–105. doi:10.1177/058310249803000201.   




Ettelaie, A., M. Layeghi, H. Zarea Hosseinabadi, and G. Ebrahimi. 2019. Prediction of Modulus of Elasticity of Poplar Wood Using Ultrasonic Technique by Applying Empirical Correction Factors. *Measurement* 135:392–9. doi:10.1016/j.measurement.2018.11.076.   




European Standard EN 1309-3 2018. 2018. Round and Sawn Timber. Methods of Measurements. Part 3: Features and Biological Degradations. Bruxelles.   

European Standard EN 13183-2. 2002. Moisture Content of a Piece of Sawn Timber. Part 2: Estimation by Electrical Resistance Method. European Committee for Standardization. Bruxelles.   

European Standard EN 14081. 2020. Timber Structures. Strength Graded Structural Timber with Rectangular Cross Section. Bruxelles.   

European Standard EN 384:2016 + A1. 2010. Structural Timber. Determination of Characteristic Values of Mechanical Properties and Density. European Committee for Standardization. Bruxelles.   


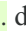


European Standard EN 408. 2011. Timber Structures. Structural Timber and Glued Laminated Timber. Determination of Some Physical and Mechanical Properties. European Committee for Standardization. Bruxelles.   





Fathi, H., S. Kazemirad, and V. Nasir. 2021. Lamb Wave Propagation Method for Nondestructive Characterization of the Elastic Properties of Wood. *Applied Acoustics* 171:107565. doi:10.1016/j.apacoust.2020.107565.   




Fernández-Serrano, Á., and A. Villasante. 2021. Longitudinal, Transverse and Ultrasound Vibration for the Prediction of Stiffness Using Models Incorporating Features in Pinus Sylvestris Timber. *European Journal of*




Wood and Wood Products 79 (6):1541–50. doi:10.1007/s00107-021-01707-0.   




Foster, R. M., and T. P. S. Reynolds. 2018. Lightweighting with Timber: An Opportunity for More Sustainable Urban Densification. *Journal of Architectural Engineering* 24 (1):1–4. doi:10.1061/(asce)ae.1943-5568.0000301.   

Genç, A. F., V. Kahya, A. C. Altunışık, M. Günaydın, and C. Demirkır. 2021. Assessment of Modal Characteristics of Cross-Laminated Timber Beams Subject to Successive Damages. *Archives of Civil and Mechanical Engineering* 21, article number: 128    

Haftka, R. T., and G. Zafer. 1992. *Elements of Structural Optimization*. Kluwer Academic Publishers. The Netherlands.    


Hassan, K. T. S., P. Horáček, and J. Tippner. 2013. Evaluation of Stiffness and Strength of Scots Pine Wood Using Resonance Frequency and Ultrasonic Techniques. *BioResources* 8 (2):1634–45. doi:10.15376/biores.8.2.1634-1645.   




Hu, H., B. T. Wang, C. H. Lee, and J. S. Su. 2006. Damage Detection of Surface Cracks in Composite Laminates Using Modal Analysis and Strain Energy Method. *Composite Structures* 74 (4):399–405. doi:10.1016/j.compstruct.2005.04.020.   





Kabir, M. F., D. L. Schmoldt, and M. E. Schafer. 2002. Time Domain Ultrasonic Signal Characterization for Defects in Thin Unsurfaced Hardwood Lumber. *Wood and Fiber Science* 34 (1):165–82.   




Kouroussis, G., L. Ben Fekih, and T. Descamps. 2017. Assessment of Timber Element Mechanical Properties Using Experimental Modal Analysis. *Construction and Building Materials* 134:254–61. doi:10.1016/j.conbuildmat.2016.12.081.   






Kovryga, A., A. Khaloian Sarnaghi, and J. W. van de Kuilen. 2020. Strength Grading of Hardwoods Using Transversal Ultrasound. *European Journal of Wood and Wood Products* 78 (5):951–60. doi:10.1007/s00107-020-01573-2.   




Liu, H., Z. Chen, Y. Liu, Y. Chen, Y. Du, and F. Zhou. 2023. Interfacial Debonding Detection for CFST Structures Using an Ultrasonic Phased Array: Application to the Shenzhen SEG Building. *Mechanical Systems and Signal Processing* 192:110214. doi:10.1016/j.ymssp.2023.110214.   

López, G., L. A. Basterra, G. Ramón-Cueto, and A. D. Diego. 2014. Detection of Singularities and Subsurface Defects in Wood by Infrared Thermography. *International Journal of Architectural Heritage* 8 (4):517–36. doi:10.1080/15583058.2012.702369.   




Lu, Z.-Q., W.-H. Liu, H. Ding, and L.-Q. Chen. 2022. Energy Transfer of an Axially Loaded Beam With a Parallel-Coupled Nonlinear Vibration Isolator. *Journal of Vibration and Acoustics* 144 (5):051009, article number: VIB-21-1389. doi:10.1115/1.4054324.    


Lu, Z.-Q., D. H. Gu, H. Ding, W. Lacarbonara, and L. Q. Chen. 2020. Nonlinear Vibration Isolation via a Circular Ring. *Mechanical Systems and Signal Processing* 136:106490. doi:10.1016/j.ymssp.2019.106490.   


Momohara, I., H. Sakai, and Y. Kubo. 2021. Comparison of Durability of Treated Wood Using Stake Tests and Survival Analysis. *Journal of Wood Science* 67, article number: 63.  doi:10.1186/s10086-021-01996-2.    




Neuenschwander, J., S. J. Sanabria, P. Schuetz, R. Widmann, and M. Vogel. 2013. Delamination Detection in a 90-Year-Old Glulam Block with Scanning Dry Point-Contact Ultrasound. *hfs* 67 (8):949–57. doi:10.1515/hf-2012-0202.   



Palma, P., and R. Steiger. 2020. Structural Health Monitoring of Timber Structures – Review of Available Methods and Case Studies. *Construction and Building Materials* 248:118528. doi:10.1016/j.conbuildmat.2020.118528.   




Perera, R., R. Marin, and A. Ruiz. 2013. Static-Dynamic Multi-Scale Structural Damage Identification in a Multi-Objective Framework. *Journal of Sound and Vibration* 332 (6):1484–500. doi:10.1016/j.jsv.2012.10.033.   

Perera, R., and A. Ruiz. 2008. A Multistage FE Updating Procedure for Damage Identification in Large-Scale Structures Based on Multiobjective Evolutionary Optimization. *Mechanical Systems and Signal Processing* 22 (4):970–91. doi:10.1016/j.ymssp.2007.10.004.   

Qu, H., T. Li, and G. Chen. 2019. Adaptive Wavelet Transform: Definition, Parameter Optimization Algorithms, and Application for Concrete Delamination Detection from Impact Echo Responses. *Structural Health Monitoring* 18 (4):1022–39. doi:10.1177/1475921718776200.   

Sanabria, S. J., R. Furrer, J. Neuenschwander, P. Niemz, and P. Schütz. 2015. Analytical Modeling, Finite-Difference Simulation and Experimental Validation of Air-Coupled Ultrasound Beam Refraction and Damping through Timber Laminates, with Application to Non-Destructive Testing. *Ultrasonics* 63:65–85. doi:10.1016/j.ultras.2015.06.013.   




Sousa, H. S., J. D. Sørensen, P. H. Kirkegaard, J. M. Branco, and P. B. Lourenço. 2013. On the Use of NDT Data for Reliability-Based Assessment of Existing Timber Structures. *Engineering Structures* 56:298–311. doi:10.1016/j.engstruct.2013.05.014.   

Sun, G., Y. Wang, Q. Luo, and Q. Li. 2022. Vibration-Based Damage Identification in Composite Plates Using 3D-DIC and Wavelet Analysis. *Mechanical Systems and Signal Processing* 173:108890. doi:10.1016/j.ymssp.2022.108890.   




Tang, S., N. Ye, and Z. Huang. 2023. Optimal Design of Flexspline Structure Based on Approximation Model. *Mechanics Based Design of Structures and Machines* 51 (3):1297–315.




doi:10.1080/15397734.2020.1864638.   




Tiitta, M., L. Tomppo, V. Möttönen, J. Marttila, J. Antikainen, R. Lappalainen, and H. Heräjärvi. 2017. Predicting the Bending Properties of Air Dried and Modified *Populus tremula* L. Wood Using Combined Air-Coupled Ultrasound and Electrical Impedance Spectroscopy. *European Journal of Wood and Wood Products* 75 (5):701–9. doi:10.1007/s00107-016-1140-0.   




Whalen, T. M. 2008. The Behavior of Higher Order Mode Shape Derivatives in Damaged, Beam-like Structures. *Journal of Sound and Vibration* 309 (3–5):426–64. doi:10.1016/j.jsv.2007.07.054.   

Wilcox, W. W. 1988. Detection of Early Stages of Wood Decay with Ultrasonic Pulse Velocity. *Forest Products Journal* 38:68–73.   


Zhai, S. Y., Y. F. Lyu, K. Cao, G. Qiang Li, W. Yong Wang, and C. Chen. 2023. Seismic Behavior of an Innovative Bolted Connection with Dual-Slot Hole for Modular Steel Buildings. *Engineering Structures* 279 (December 2022):115619. doi:10.1016/j.engstruct.2023.115619.   

Zhang, C. W. 2023. The Active Rotary Inertia Driver System for Flutter Vibration Control of Bridges and Various Promising Applications. *Science China Technological Sciences* 66 (2):390–405. doi:10.1007/s11431-022-2228-0.   

Zhang, Z., W. Li, and J. Yang. 2021. Analysis of Stochastic Process to Model Safety Risk in Construction Industry. *Journal of Civil Engineering and MANAGEMENT* 27 (2):87–99. doi:10.3846/jcem.2021.14108.   


Zhang, Z., G. Liang, Q. Niu, F. Wang, J. Chen, B. Zhao, and L. Ke. 2022. A Wiener Degradation Process with Drift-Based Approach of Determining Target Reliability Index of Concrete Structures. *Quality and Reliability Engineering International* 38 (7):3710–25. doi:10.1002/qre.3168.   

Author Query


1. **Query [AQ0]** : Please review the table of contributors below and confirm that the first and last names are structured correctly and that the authors are listed in the correct order of contribution. This check is to ensure that your names will appear correctly online and when the article is indexed. 

Sequence	Prefix	Given name(s)	Surname	Suffix
1		Ramon	Sancibrian	
2		Ignacio	Lombillo	
3		Rebeca	Sanchez	
4		Alvaro	Gaute-Alonso	


Response by Author: "Ok"

2. **Query [AQ1]** : Please reduce your abstract to not more than 100 words, as per style sheet requirement. 


Response by Author: "Answered within text"

3. **Query [AQ2]** : There is no mention of (European Standard EN 1309-3 2018 and European Standard EN 3842016 + A1 2010) in the text. Please insert a citation in the text or delete the reference as appropriate. 


Response by Author: "The European standard EN 1309-3 is mentioned in section 2.2 of the text, specifically in the first sentence regarding visual grading. The correct year of reference is 2018, not 2011 as previously stated. This change has been made accordingly. Furthermore, in section 2.3, the European standard EN 384 2016 +A1 is mentioned. However, the correct year of publication is 2020, not 2010. This correction has been applied to both the text and the references list."

4. **Query [AQ3]** : Please provide missing publisher location for the "European Standard EN 408., 2011" references list entry. 


Response by Author: "The publisher location of all European standards have been corrected."

5. **Query [AQ4]** : Please provide missing page range for the "Genç et al., 2021" references list entry. 


Response by Author: "This paper has 21 pages. However, the publisher of this journal does not provide the page range for its articles. Instead, the journal cites this article with the following reference:Genç, A.F., Kahya, V., Altunışık, A.C. et al. Assessment of modal characteristics of cross-laminated timber beams subject to successive damages. Archiv.Civ.Mech.Eng 21, article number: 128 (2021). <https://doi.org/10.1007/s43452-021-00288-2>
The article number has been included."

6. **Query [AQ5]** : Please provide missing publisher location for the "Haftka and Zafer, 1992" references list entry. 

Response by Author: "Answered within text"

7. **Query [AQ6]** : Please provide missing page range for the "Lu et al., 2022" references list entry. 


Response by Author: "The article consists of 12 pages. However, the publisher's citation structure does not include the page range, and the article itself does not provide specific page numbers. The journal itself provides the citation as follows:J. Vib. Acoust. Oct 2022, 144(5): 051009, article number: VIB-21-1389.The reference to the article number has been added to the paper.
"

8. **Query [AQ7]** : Please provide missing page range for the "Momohara et al., 2021" references list entry. 


Response by Author: "The article consists of 8 pages. However, the publisher's citation structure does not indicate the page range, and the article itself does not provide specific page numbers. The citation provided by the journal is as follows:
Momohara, I., Sakai, H. & Kubo, Y. Comparison of durability of treated wood using stake tests and survival analysis. J Wood Sci 67, article number 63 (2021).
<https://doi.org/10.1186/s10086-021-01996-2>
The article number has been included."


9. **Query [AQ8]** : Please note that the ORCID section has been created from information supplied with your manuscript submission/CATS. Please correct if this is inaccurate. 


Response by Author: "Ok"


10. **Query [AQ9]** : Please provide physical address of the corresponding author. 
- Response by Author:** "The physical address of the corresponding author is the following:
ETS of Industrial and Telecommunication Engineers, Department of Structural and Mechanical Engineering, University of Cantabria, Cantabria, Spain"


Comments


1. **Comment by Author:** "The parenthesis ")" and the comma "," are not part of the equation. " 
- [AUTHOR: RAMON SANCIBRIAN - 7/8/2023 12:32:40 PM]


2. **Comment by Author:** "The period "." is not part of the equation. " 
- [AUTHOR: RAMON SANCIBRIAN - 7/8/2023 12:38:12 PM]











3. **Comment by Author:** "The comma "," is not part of the equation. " 
- [AUTHOR: RAMON SANCIBRIAN - 7/8/2023 12:39:19 PM]

4. **Comment by Author:** "The comma "," is not part of the equation. " 
- [AUTHOR: RAMON SANCIBRIAN - 7/8/2023 12:39:39 PM]

5. **Comment by Author:** "The comma "," is not part of the equation. " 
- [AUTHOR: RAMON SANCIBRIAN - 7/8/2023 12:40:01 PM]

6. **Comment by Author:** "The comma "," is not part of the equation. " 
- [AUTHOR: RAMON SANCIBRIAN - 7/8/2023 12:40:16 PM]

7. **Comment by Author:** "The period "." is not part of the equation. " 
- [AUTHOR: RAMON SANCIBRIAN - 7/8/2023 12:40:42 PM]

8. **Comment by Author:** "The comma "," is not part of the equation. "
[AUTHOR: RAMON SANCIBRIAN - 7/8/2023 12:40:55 PM] 
9. **Comment by Author:** "The comma "," is not part of the equation. "
[AUTHOR: RAMON SANCIBRIAN - 7/8/2023 12:41:08 PM] 
10. **Comment by Author:** "The period "." is not part of the equation. "
[AUTHOR: RAMON SANCIBRIAN - 7/8/2023 12:41:28 PM] 
11. **Comment by Author:** "The comma "," is not part of the equation. "
[AUTHOR: RAMON SANCIBRIAN - 7/8/2023 12:41:40 PM] 
12. **Comment by Author:** "The comma "," is not part of the equation. "
[AUTHOR: RAMON SANCIBRIAN - 7/8/2023 12:41:59 PM] 
13. **Comment by Author:** "The comma "," is not part of the equation. "
[AUTHOR: RAMON SANCIBRIAN - 7/8/2023 12:42:25 PM] 
14. **Comment by Author:** "The period "." is not part of the equation. "
[AUTHOR: RAMON SANCIBRIAN - 7/8/2023 12:42:46 PM] 
15. **Comment by Author:** "The comma "," is not part of the equation. "
[AUTHOR: RAMON SANCIBRIAN - 7/8/2023 12:43:13 PM] 
16. **Comment by Author:** "The period "." is not part of the equation. "
[AUTHOR: RAMON SANCIBRIAN - 7/8/2023 12:43:33 PM] 
17. **Comment by Author:** "The comma "," is not part of the equation. "


[AUTHOR: RAMON SANCIBRIAN - 7/8/2023 12:43:51 PM]

18. **Comment by Author:** "The period "." is not part of the equation. "



[AUTHOR: RAMON SANCIBRIAN - 7/8/2023 12:44:21 PM]

19. **Comment by Author:** "The comma "," is not part of the equation. "



[AUTHOR: RAMON SANCIBRIAN - 7/8/2023 12:44:34 PM]

20. **Comment by Author:** "The comma "," is not part of the equation. "



[AUTHOR: RAMON SANCIBRIAN - 7/8/2023 12:44:55 PM]

21. **Comment by Author:** "The period "." is not part of the equation. "



[AUTHOR: RAMON SANCIBRIAN - 7/8/2023 12:45:15 PM]

22. **Comment by Author:** "The period "." is not part of the equation. "



[AUTHOR: RAMON SANCIBRIAN - 7/8/2023 12:45:40 PM]

23. **Comment by Author:** "In the Figure 12 caption, the comma "," after Est^s, and the comma "," after Eus^s are not part of the equation. "



[AUTHOR: RAMON SANCIBRIAN - 7/8/2023 12:54:48 PM]

24. **Comment by Author:** "The period "." is not part of the equation. "



[AUTHOR: RAMON SANCIBRIAN - 7/8/2023 12:55:34 PM]

25. **Comment by Author:** "The period "." is not part of the equation. "



[AUTHOR: RAMON SANCIBRIAN - 7/8/2023 12:56:13 PM]

26. **Comment by Author:** "The period "." is not part of the equation. "



[AUTHOR: RAMON SANCIBRIAN - 7/8/2023 12:56:38 PM]

27. **Comment by Author:** "The comma "," is not part of the equation. "

[AUTHOR: RAMON SANCIBRIAN - 7/8/2023 12:56:50 PM]



28. **Comment by Author:** "The full stop "." is not part of the equation. "

[AUTHOR: RAMON SANCIBRIAN - 7/8/2023 12:57:38 PM]



29. **Comment by Author:** "The comma "," is not part of the equation. "

[AUTHOR: RAMON SANCIBRIAN - 7/8/2023 12:57:52 PM]



30. **Comment by Author:** "The period "." is not part of the equation. "

[AUTHOR: RAMON SANCIBRIAN - 7/8/2023 12:58:18 PM]



31. **Comment by Author:** "The comma "," is not part of the equation. "

[AUTHOR: RAMON SANCIBRIAN - 7/8/2023 12:58:32 PM]



32. **Comment by Author:** "The period "." is not part of the equation. "

[AUTHOR: RAMON SANCIBRIAN - 7/8/2023 12:58:50 PM]



33. **Comment by Author:** "The period "." is not part of the equation. "

[AUTHOR: RAMON SANCIBRIAN - 7/8/2023 12:59:10 PM]



34. **Comment by Author:** "The comma "," is not part of the equation. "

[AUTHOR: RAMON SANCIBRIAN - 7/8/2023 12:59:35 PM]



35. **Comment by Author:** "The comma "," is not part of the equation. "

[AUTHOR: RAMON SANCIBRIAN - 7/8/2023 12:59:42 PM]



36.

Comment by Author: "The comma "," is not part of the equation. "



[AUTHOR: RAMON SANCIBRIAN - 7/8/2023 12:59:55 PM]

37.

Comment by Author: "The period "." is not part of the equation. "



[AUTHOR: RAMON SANCIBRIAN - 7/8/2023 1:00:09 PM]